nature communications

Article

https://doi.org/10.1038/s41467-026-71873-3

PEX11 mediates intralumenal vesicle formation in peroxisomes

Received: 18 December 2025

Accepted: 1 April 2026

Published online: 21 April 2026

Check for updates

Nathan E. Tharp, Chelsea An, James Hwang, Nayeli S. Shad, Zachary J. Wright & Bonnie Bartel

Peroxisomes are eukaryotic organelles that compartmentalize crucial metabolic reactions. Peroxisome size, shape, and number are governed by the peroxisomal membrane protein PEX11. PEX11 is encoded in multiple isoforms across diverse eukaryotes, including five in Arabidopsis, but the functional distinctions among these isoforms are largely uncharacterized. Here we report null *pex11* mutants in plants expressing reporters that mark peroxisome membranes and lumen to illuminate distinct functions for PEX11 isoforms. We find that PEX11C/D/E promotes the formation of peroxisomal intralumenal vesicles, limits peroxisome size throughout development, and is required for efficient fatty acid β-oxidation in germinating seedlings. Unlike the pervasive roles of PEX11C/D/E, we find that PEX11A/B promotes the formation of peroxisomal intralumenal vesicles and limits peroxisome enlargement specifically during seedling lipid mobilization. Complete loss of the PEX11 family confers seedling lethality, even though peroxisomes remain abundant. Our findings reveal that Arabidopsis PEX11 isoforms shape internal peroxisome membranes and have distinct functions in cellular physiology that are essential for plant development. These results extend the roles of PEX11 beyond its canonical function in peroxisome division.

Peroxisomes are metabolically plastic organelles that compartmentalize specialized metabolism. In addition to reactive oxygen species catabolism and fatty acid β-oxidation[1], peroxisomes harbor various reactions, depending on the organism or tissue, including plasmalogen synthesis in mammals[2] and phytohormone maturation in plants[1]. Most multicellular organisms cannot survive without peroxisomes. For example, human peroxisome biogenesis disorders can be lethal in infancy[3,4], and plant peroxisomes are essential for embryogenesis and for catabolizing the fats stored in lipid droplets that fuel early seedling development[1].

New peroxisomes arise from the endoplasmic reticulum[5,6] or are generated from pre-existing peroxisomes via division[7–9]. The proteins required for peroxisome biogenesis, division, and import of membrane and lumenal proteins are known as peroxins (PEX proteins), and a core set of peroxins is conserved among metazoans, fungi, and plants[10]. In lumenal protein import, cytosolic receptor peroxins bind to peroxisome targeting signals (PTSs) on proteins destined for the peroxisome lumen and accompany their cargo into the organelle, with the assistance of membrane-embedded peroxins, before exiting to facilitate further import rounds[1,11,12].

A prominent, conserved peroxin implicated in peroxisome division is PEX11. PEX11 is a transmembrane protein thought to coordinate peroxisomal division by tubulating the membrane[13,14] and recruiting the fission machinery that executes scission[9,11,15–18]. The N-terminal domain of *Penicillium chrysogenum* PEX11 can induce liposome tubulation[14], and *Saccharomyces cerevisiae* (baker's yeast) and *Physcomitrella patens* (moss) *pex11* mutants contain fewer, larger peroxisomes, consistent with fission defects[19–21]. Similarly, downregulating *Arabidopsis thaliana PEX11* transcripts using RNA interference diminishes peroxisome number and increases peroxisome size[16,22,23].

[1]Biosciences Department, Rice University, Houston, TX, USA. [2]Present address: School of Medicine, University of Texas Southwestern Medical Center, Dallas, TX, USA. [3]Present address: Department of Public Health Sciences, Biological Sciences Division, The University of Chicago, Chicago, IL, USA. [4]Present address: Janelia Research Campus, Howard Hughes Medical Institute, Ashburn, VA, USA. e-mail: bartel@rice.edu

Conversely, overexpressing human[13,24–26], plant[13,16,23,27], or yeast[13,28] PEX11 isoforms can induce peroxisome tubulation or increase peroxisome abundance.

Unlike other peroxins, all examined eukaryotes with peroxisomes encode multiple PEX11 isoforms[10,29], including five in Arabidopsis (PEX11A-E), three in *S. cerevisiae* (Pex11, Pex25, and Pex27), and three in humans (PEX11α, β, and γ). Yeast mutants lacking individual PEX11 isoforms display enlarged peroxisomes, and the removal of all three homologs impairs import of peroxisomal enzymes[19,20]. PEX11β, the most prominent mammalian isoform, alters peroxisome abundance[25] and is critical for neuronal function[30] and epidermal cell differentiation[31], whereas PEX11α is dispensable for peroxisome function[32], and PEX11γ overexpression does not alter peroxisome abundance[32]. However, how various PEX11 isoforms function individually and in combination remains incompletely understood.

There may be roles for PEX11 beyond peroxisome division. Peroxisomes are born from complex ER "nest" domains[6], a process that presumably requires the severing of nascent organelles from the ER, and PEX11 has been implicated in de novo peroxisome formation in fungi[29]. Moreover, vesicles within peroxisomes are observed in plants[6,33–36], yeast[37,38], and animals[39,40]. We recently used fluorescent reporters separately labeling peroxisomal membranes and lumen to visualize intralumenal vesicle (ILV) formation[36] and peroxisome biogenesis from ER nests[6] in Arabidopsis seedlings. Peroxisomal ILVs form via endosomal sorting complex required for transport (ESCRT)-assisted invagination of the outer membrane and are hypothesized to aid in mobilizing fats stored in lipid droplets[36]. However, the full mechanism of ILV formation, including the peroxisome-specific components, remains unknown.

In this study, we discovered unanticipated roles for PEX11 in peroxisome biology by examining various combinations of null *pex11* mutants in Arabidopsis, an ideal model for elucidating peroxisome structure and function. Arabidopsis seedlings are well-suited to live-cell microscopy and contain remarkably large peroxisomes compared to yeast or mammals[36,41], allowing visualization of peroxisome substructures using light microscopy[36]. Moreover, quantitative physiological assays can report peroxisome function in intact seedlings[42]. We found that disrupting various combinations of PEX11 isoforms conferred enlarged peroxisomes lacking ILVs, failure to mobilize stored fats, and severe physiological defects, including seedling death. Our data reveal that PEX11 isoforms have distinct and overlapping membrane-shaping roles beyond peroxisome fission in Arabidopsis.

Results

PEX11 promotes peroxisomal ILV formation and limits peroxisome size

Disrupting PEX11 increases peroxisome size in various systems, including yeast[19,28,43] and plants[16,21–23]. Given our discovery of pervasive ILVs in Arabidopsis peroxisomes[36], the involvement of PEX11 in membrane shaping, and the recent connection of PEX11 to an ESCRT component[44], we sought to determine whether PEX11 might function in ILV formation in addition to its canonical role in peroxisome division.

As in other eukaryotes, PEX11 is encoded in a multigene family in Arabidopsis[10]. PEX11A-B and PEX11C-E form distinct subfamilies (Supplementary Fig. 1a, b)[22,23] with similar predicted structures (Supplementary Fig. 1e, f). The primary sequences of PEX11C, PEX11D, and PEX11E are over 80% identical to each other, whereas PEX11A and PEX11B are ~29% identical to each other and less similar to members of the PEX11C-E clade (Supplementary Fig. 1). To explore the roles of these subfamilies, we separately generated *PEX11A-B* or *PEX11C-E* null mutations using a plant-optimized CRISPR-Cas9 system[45] to simultaneously express two or three guide RNAs (gRNAs) (Supplementary Fig. 1d). To enable visualization of peroxisome lumen and membrane, we generated mutations in plants carrying a transgene constitutively expressing mRuby3 fused to a C-terminal PTS1 (mRuby3-PTS1) and mNeonGreen fused to the C-terminal membrane anchor of PEX26 (mNeonGreen-mPTS^{PEX26})[36] (Fig. 1a). From the progeny of the Cas9/gRNA-expressing plants, we obtained various single and higher-order *pex11* mutants carrying early frameshift mutations (Supplementary Table 1, 2) and lacking the Cas9 transgene. Immunoblot analysis using an antibody raised to a conserved region of PEX11E[46] revealed the expected ~27-kDa protein in *pex11cd*, *pex11 de*, and *pex11abce* mutants but not in the *pex11cde* mutant (Fig. 2a, Supplementary Fig. 2a, b). These data indicate that the antibody recognizes all isoforms in the PEX11C/D/E clade and confirm that our *pex11c*, *pex11d*, and *pex11e* frameshift mutations (Supplementary Table 1, 2) prevent accumulation of the corresponding full-length proteins.

We compared peroxisomes in the parental wild-type reporter line with those in the *pex11a pex11b* double mutant, henceforth referred to as *pex11ab*, and a mutant lacking the other three PEX11 proteins (*pex11c pex11d pex11e*; *pex11cde*). We imaged the abundant peroxisomes in cotyledons, embryonic leaves packed with lipid droplets that fuel seedling growth before photosynthesis begins, and found dramatically enlarged peroxisomes when either subset of *PEX11* genes was disrupted (Fig. 1b, c).

As wild-type seedlings develop, cotyledon peroxisomes enlarge as lipid stores are mobilized and then shrink as lipid stores are depleted (Fig. 1d-f)[36,41]. In our analysis, wild-type peroxisomes expanded from an average diameter of about 3 μm at day 2 to 5 μm at day 3 before returning to 3 μm by day 7 (Fig. 1d-f). Similarly, *pex11ab* peroxisomes expanded as seedlings developed and were smaller again by day 7 (Fig. 1d-f). However, *pex11ab* peroxisomes attained markedly larger maximum sizes than wild-type peroxisomes, with almost half of *pex11ab* peroxisomes exceeding 10 μm in diameter at day 5 (Fig. 1d-f). To determine whether the restoration of smaller peroxisomes in older *pex11ab* seedlings reflected shrinkage of individual peroxisomes, we followed peroxisomes in *pex11ab* mutants using time-lapse microscopy. In 3-day-old hypocotyls, we observed individual *pex11ab* peroxisomes shrinking over time (Fig. 1i, Supplementary Movie 1). In contrast to wild-type and *pex11ab* peroxisomes, the dramatic enlargement of *pex11cde* peroxisomes continued throughout the time course. Remarkably, peroxisomes in older *pex11cde* cotyledons sometimes exceeded 20 μm in diameter (Fig. 1d-f). Although these enlarged peroxisomes remained mostly spherical (Supplementary Fig. 2f), some were misshapen due to limitations imposed by the surrounding cell walls (Fig. 1d, asterisks).

Strikingly, ILVs were less apparent or absent in the large peroxisomes of higher-order *pex11* mutants. As seedlings matured, the enlarged peroxisomes in *pex11ab* and *pex11cde* contained notably sparse ILVs, and the few internal membranes that remained often appeared to be tiny ILVs or membrane remnants (Fig. 1c, d). However, the lack of PEX11A/B or PEX11C/D/E did not completely block ILV formation, as the small peroxisomes found in very young (2-day) *pex11* mutant seedlings appeared to contain internal membranes (Fig. 1d), and *pex11ab* peroxisomes appeared to acquire internal membranes as they shrank (Fig. 1i, Supplementary Movie 1).

Because the *pex11ab* and *pex11cde* mutants displayed such dramatic peroxisome phenotypes (Fig. 1), we also examined other allele combinations. We found similarly increased peroxisome size and reduced internal membrane content in multiple different *pex11a pex11b* allele combinations (Supplementary Fig. 2c). Moreover, cotyledons of *pex11a* and *pex11b* single mutants sometimes displayed slightly enlarged peroxisomes that appeared to have fewer ILVs than wild-type peroxisomes (Supplementary Fig. 2d, e). However, this expansion was not as extensive as in the *pex11ab* double mutants (Supplementary Fig. 2c-e), indicating that PEX11A and PEX11B are partially redundant. In contrast, peroxisomes in *pex11cd* and *pex11de* mutants resembled wild type rather than *pex11cde* in both size and ILV content (Supplementary Fig. 2d), indicating that PEX11C, D, and E function redundantly.

https://doi.org/10.1038/s41467-026-71873-3

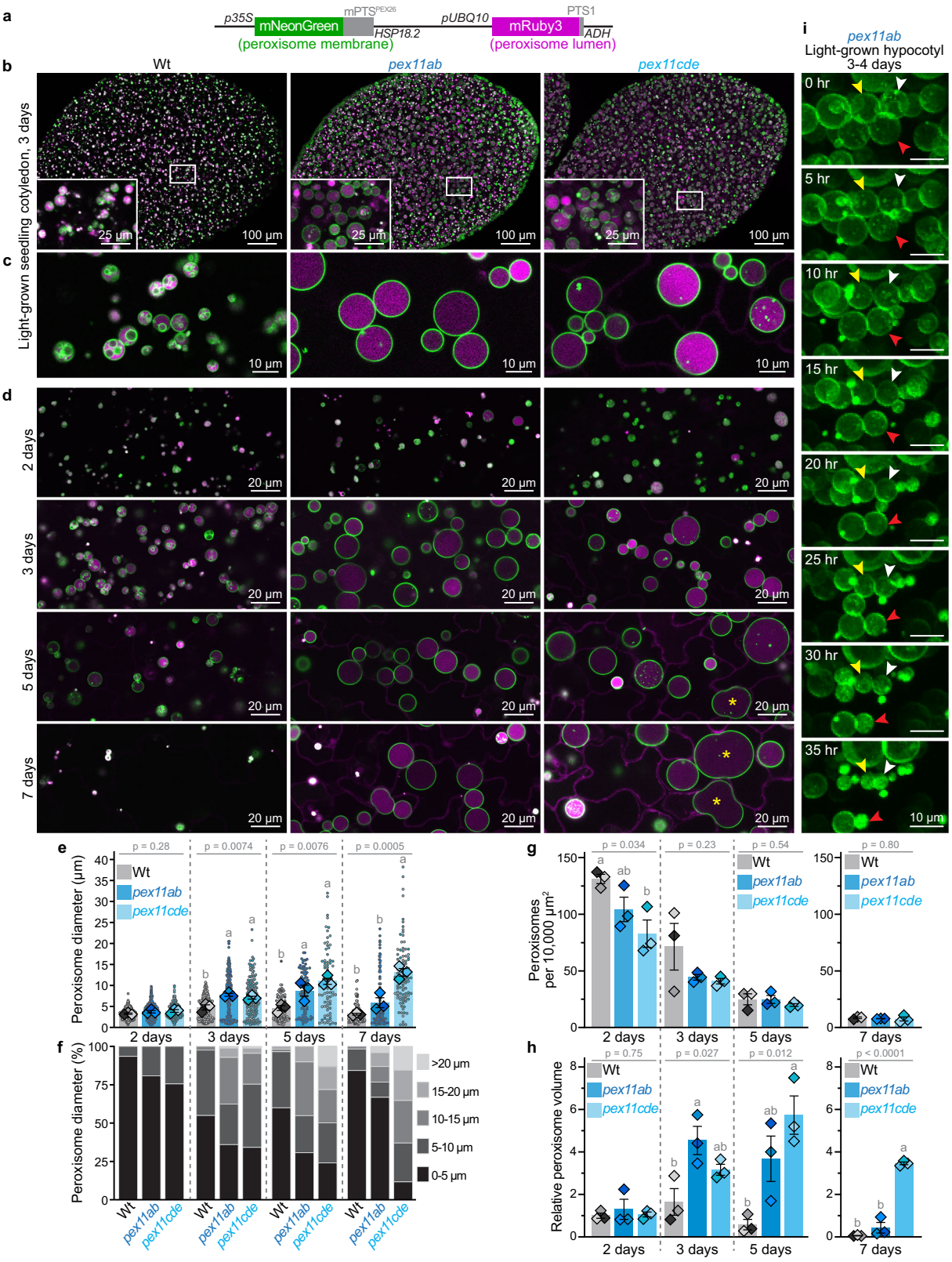

Large peroxisomes could result from reduced ILV formation (because ILVs form from the outer peroxisomal membrane[6,36]) or from decreased peroxisome division, which would presumably decrease peroxisome numbers. Although we did observe fewer peroxisomes in cotyledons and hypocotyls of 2- or 3-day-old *pex11cde* mutants than in wild type or *pex11ab* (Fig. 1g, Supplementary Fig. 4c), we did not find significantly altered peroxisome numbers in older *pex11* cotyledons (Fig. 1g), suggesting that PEX11-mediated fission cannot explain all *pex11* phenotypes. Moreover, the total volume occupied by peroxisomes in cotyledons of 3-day-old *pex11ab* mutants and 5- and 7-day-old *pex11cde* mutants was dramatically elevated (Fig. 1h), which is inconsistent with defects in fission alone. We concluded that both PEX11A/B and PEX11C/D/E limit peroxisome size during seedling development by supporting peroxisomal ILV formation.

https://doi.org/10.1038/s41467-026-71873-3

Fig. 1 | Arabidopsis *PEX11* genes control peroxisome size and ILV content. **a** *pex11* mutations were generated in plants expressing mNeonGreen-mPTS^{PEX26} and mRuby3-PTS1 reporters to visualize the peroxisome membrane and lumen, respectively. **b** Confocal images of peroxisomes in cotyledons of 3-day-old seedlings expressing the reporters diagrammed in **a**. Maximum-intensity projections composed of 25 slices taken at 2.5-µm steps of entire cotyledons with magnified inlays are shown. **c** Higher magnification single-slice images of peroxisomes. **d** Confocal images of peroxisomes in cotyledons of 2- to 7-day-old seedlings. Asterisks indicate non-spherical peroxisomes in *pex11cde* that appear to be confined by the surrounding cell walls. **e**–**h** Quantification of peroxisome size (**e, f**), peroxisome number (**g**), and relative total peroxisome volume (**h**) in cotyledons of 2- to 7-day-old seedlings. Individual peroxisome diameters (dots) from three seedlings are shown in three shades of gray, dark blue, or light blue; bars represent means of the three replicate means (diamonds); and error bars represent SEM. Letters above bars represent homologous subsets from Tukey's post-hoc test when p-values were <0.05 following separate one-way ANOVA tests comparing each genotype at each time point. The lack of shared letters indicates a significant difference between the means. The stacked bar chart (**f**) depicts the mean percent of peroxisomes with the indicated diameters from three replicates. Peroxisome number and volume (**g, h**) are plotted separately for 7-day-old seedlings because larger z-stacks were used for quantification (see Methods). **i** Stills from a 42-hour time-lapse movie (Supplementary Movie 1) showing *pex11ab* mutant peroxisomes shrinking as they acquire internal membranes. Differently colored arrowheads track individual peroxisomes over 35 hours.

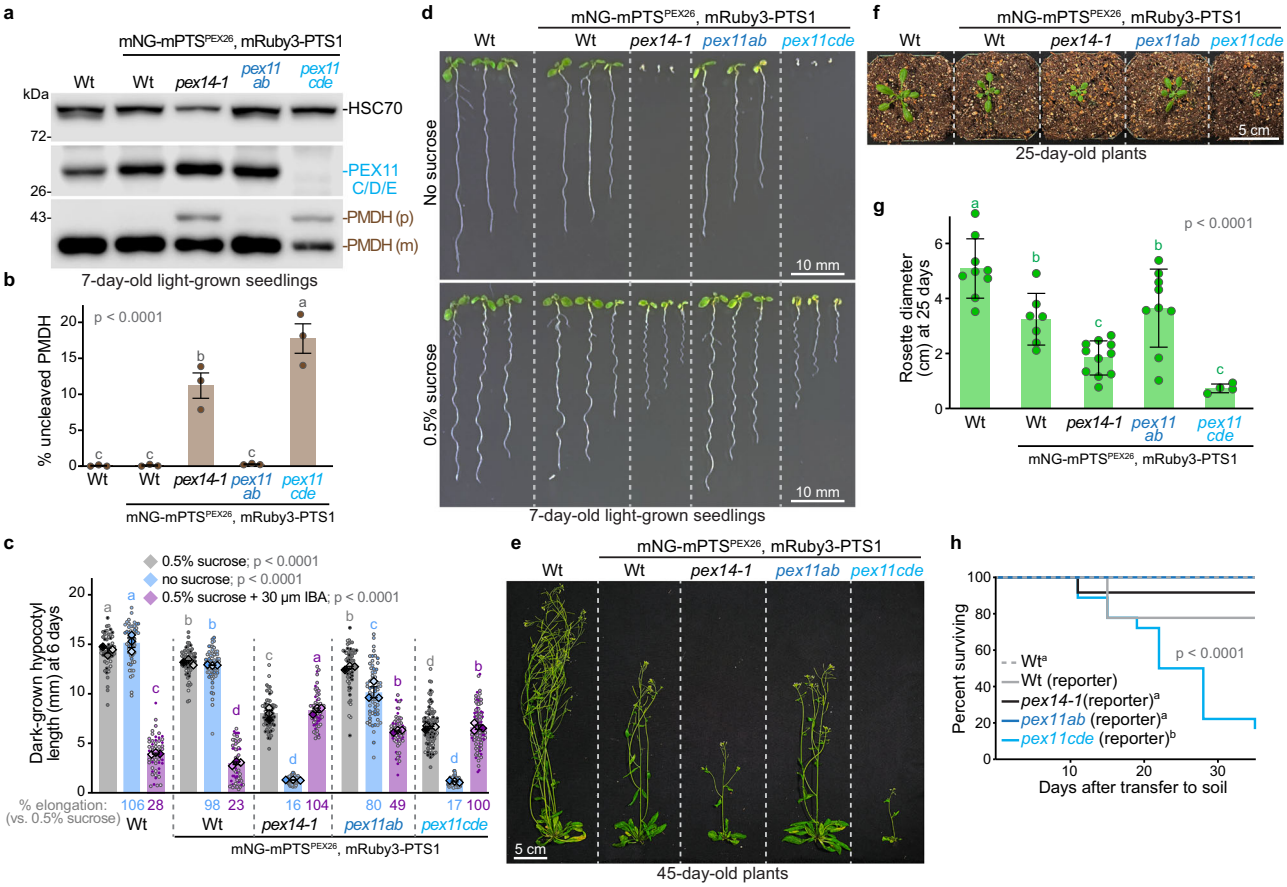

Fig. 2 | PEX11 isoforms differentially contribute to plant development and physiology. **a** Immunoblots of sucrose-grown seedlings probed with the indicated antibodies. HSC70 is a loading control. The positions of molecular mass markers (in kDa) are shown on the left. The PMDH2 precursor (p) is cleaved into the mature protein (m) after import into the peroxisome lumen. **b** The percentage of precursor PMDH versus total PMDH from three biological replicates, including the one shown in **a**. **c** *pex11cde* seedlings display IBA-resistant elongation and growth defects that are partially restored by sucrose supplementation. Dark-grown hypocotyl lengths of individual seedlings (dots) from three biological replicates are shown in three shades of gray, blue, or purple; bars represent means of the replicates (diamonds). **d** *pex11cde* seedling growth defects are partially restored by sucrose supplementation. **e** Representative plants after the transition to flowering. **f** Representative plants after transfer to soil. **g** Bars represent mean rosette diameters of individual plants (dots), which included 9, 7, 11, 9, or 4 plants for Wt, Wt reporter, *pex14-1*, *pex11ab*, or *pex11cde*, respectively. **h** Survival plot of wild-type and mutant plants. 8-day-old seedlings were transferred to soil, and survival was monitored for 35 days. The Mantel-Cox (log-rank) test was used to compare survival curves using pairwise comparison between each genotype compared to the wild-type reporter. p-values were adjusted using Bonferroni correction. The lack of shared letters indicates a significant difference between the distributions. In **b, c**, and **g**, letters above bars represent homologous subsets assigned by Tukey's post-hoc test when one-way ANOVA p-values were <0.05. In **c**, separate one-way ANOVA tests were performed to compare genotypes at each condition. The lack of shared letters indicates a significant difference between the means. Error bars represent SEM (**b, c**) or SD (**g**).

PEX11C/D/E facilitates lipid mobilization, plant growth, and peroxisomal protein import

To assess the protein import competence of the aberrant *pex11* peroxisomes, we compared our mutants to wild type and *pex14-1*, a mutant with a frameshift mutation near the middle of the *PEX14* gene that prevents accumulation of full-length PEX14 and efficient lumenal protein import (Supplementary Fig. 2a, 4a)[47]. As a quantitative proxy for import, we monitored the processing of a PTS2-containing protein, peroxisomal malate dehydrogenase (PMDH). Because the N-terminal PTS2 region is removed in peroxisomes, mutants with inefficient import accumulate the cytosolic precursor protein, which can be visualized by immunoblotting[48–50]. We found that, like *pex14*[47],

pex11cde displayed incomplete PMDH processing (Fig. 2a, b), suggesting that PEX11C/D/E directly or indirectly supports lumenal protein import.

To evaluate the metabolic competence of *pex11* peroxisomes, we used peroxisome-related physiological assays. Peroxisomes are the sole site of β-oxidation in plants[51], and dysfunctional peroxisomes inefficiently access fixed carbon stored in lipid droplets, conferring reduced seedling growth that can be partially restored by the provision of sucrose[52,53]. The wild-type reporter line displayed slightly reduced growth compared to untransformed Arabidopsis (Fig. 2c-g), whereas *pex11cde* mutants displayed compromised growth in both the light and the dark that was partially rescued by sucrose supplementation (Fig. 2c, d, Supplementary Fig. 3a, b). The *pex11cde* growth defects resembled those of *pex14-1*, suggesting reduced peroxisome function. In contrast, the *pex11a*, *pex11b*, *pex11ab*, *pex11cd*, and *pex11de* seedlings had at most mild growth defects compared to the parental line (Fig. 2c, d, Supplementary Fig. 3a). The *pex11cde* growth defects persisted into adulthood and were generally more severe than those displayed by *pex14*. For example, *pex11cde* plants had small rosettes, short stature, and decreased survival after transplantation to soil (Fig. 2e-h). In contrast, *pex11ab* resembled the parental line in these assays (Fig. 2e-h). We concluded that the PEX11C/D/E clade, unlike PEX11A/B, is required throughout plant development.

In a second readout of peroxisome metabolism, we monitored responses to a phytohormone precursor, indole-3-butyric acid (IBA). Because peroxisomes β-oxidize IBA into active auxin, which inhibits root[53] and hypocotyl elongation[54], and promotes lateral root formation[53], peroxisomal dysfunction limits IBA responsiveness. Like *pex14*, the IBA responsiveness of the *pex11cde* mutant was clearly impaired; *pex11cde* hypocotyls and primary roots elongated similarly with or without IBA supplementation (Fig. 2c, Supplementary Fig. 3a, b). In contrast, various single and double *pex11* mutants had negligible defects in these assays (Supplementary Fig. 3a), and *pex11ab* hypocotyls were only slightly less IBA-responsive than the wild-type reporter line (Fig. 2c, Supplementary Fig. 3a, b). When we monitored lateral root promotion by IBA, *pex11ab* resembled the parental line, whereas *pex11cde* displayed intermediate IBA responsiveness compared to *pex14*, which did not generate lateral roots in response to IBA (Supplementary Fig. 3c). The severe physiological defects of *pex11cde* and the minor defects of *pex11ab* (Fig. 2) suggest that the two PEX11 clades have distinct roles despite both mutants displaying enlarged cotyledon peroxisomes (Fig. 1).

Arabidopsis peroxisomes expand during seedling development[36,41]. This enlargement requires the transfer of fats from lipid droplets, as peroxisomes in mutants lacking the PXA1 (ABCD1) fatty acid transporter remain small during seedling development[36]. Similarly, peroxisomes in a mutant lacking SDP1, a prominent triacylglycerol (TAG) lipase[55], were smaller than wild-type peroxisomes during seedling development (Supplementary Fig. 4a). In contrast, mutants lacking certain fatty acid β-oxidation enzymes accumulate excessively expanded peroxisomes during seedling development, with some of these mutants exhibiting no marked physiological defects[36,41,52,56,57]. Because *pex11ab* and *pex11cde* mutants both displayed large peroxisomes (Fig. 1), but only *pex11cde* showed physiological defects associated with inefficient lipid mobilization (Fig. 2), we monitored lipid droplet utilization in *pex11* mutants. We found abundant lipid droplets in *pex11* mutants and wild-type cotyledons at 3 days, but by 7 days, when lipid droplets were sparse in wild-type and *pex11ab* cotyledons, numerous lipid droplets remained in *pex11cde* mutants (Fig. 3a). Moreover, OLEOSIN1 (OLE1), a lipid droplet coat protein that is degraded as lipids are mobilized[58,59], remained abundant in 7-day-old *pex11cde* and *pex14* seedlings after it had been degraded in wild type (Fig. 3b, c). We quantified lipid retention by monitoring seedling TAG levels using thin-layer chromatography. Unlike in *pex11ab*, we observed elevated TAG levels in 5- and 7-day-old *pex11cde* seedlings compared to wild type (Fig. 3d). To assess the global impacts of PEX11 on seedling lipids, we used lipidomics (Supplementary Fig. 5). Lipid content was not notably altered in 7- or 12-day-old *pex11ab* seedlings (Fig. 3e, Supplementary Fig. 5a, 6). In contrast, the chloroplast membrane lipids digalactosyldiacylglycerol (DGDG) and monogalactosyldiacylglycerol (MGDG) were reduced in older *pex11cde* seedlings (Fig. 3e, Supplementary Fig. 5, 6), commensurate with the delayed development of this mutant (Fig. 2). Most notably, 7- and 12-day-old *pex11cde* seedlings, like *sdp1* and *pex14*, had markedly elevated TAG and diacylglycerol (DAG) levels compared to the wild-type reporter line (Fig. 3e, Supplementary Fig. 5, 6). Intriguingly, 12-day-old *pex11cde* seedlings also had moderately increased levels of the membrane lipid phosphatidylcholine (PC), an alteration that was not observed in *sdp1* or *pex14* mutants (Fig. 3e, Supplementary Fig. 5, 6). Together with the sucrose dependence of *pex11cde* (Fig. 2c, d), these findings confirm that PEX11C/D/E is needed for efficient lipid mobilization during seedling development, whereas PEX11A/B makes at most minor contributions to this process.

PEX11A/B promotes ILV formation and restrains peroxisome size during lipid mobilization

We directly tested whether lipid mobilization was necessary for the extreme peroxisome expansion observed in *pex11* mutants by inhibiting lipid mobilization with diphenyl methylphosphonate (DMP)[60]. We found that wild-type and *pex11ab* seedlings grown on DMP contained more abundant lipid droplets (Supplementary Fig. 4b) than mock-treated seedlings, confirming that DMP impaired lipid mobilization (Fig. 4a). These lipid droplet differences were not apparent in *pex11cde* mutants (Supplementary Fig. 4b), which already displayed impaired TAG mobilization (Fig. 3). Peroxisome numbers were unaffected when seedlings were grown on DMP (Supplementary Fig. 3c), suggesting that the lipid mobilization inhibitor does not impact peroxisome proliferation. Strikingly, DMP fully suppressed peroxisome enlargement in both *pex11ab* and wild-type seedlings (Fig. 4b, c). In marked contrast, *pex11cde* peroxisome size was unaffected by DMP (Fig. 4b, c).

To confirm that lipid mobilization drives *pex11ab* peroxisome enlargement, we genetically disabled lipid mobilization in our reporter line and the *pex11ab* mutant. We used CRISPR-Cas9 to introduce frameshift mutations in the genes encoding three lipid mobilization enzymes (Fig. 4a): SDP1, a TAG lipase[55]; PXA1, the peroxisomal fatty-acyl-CoA transporter[61,62]; or PED1, a thiolase acting in β-oxidation[52]. We found that 3-day-old *sdp1*, *pxa1*, and *ped1* seedlings contained smaller peroxisomes than wild type or *pex11ab* (Fig. 4d). Moreover, when *pex11ab* mutants lacked PXA1 or PED1, peroxisome enlargement was markedly diminished (Fig. 4d). Similarly, when *pex11ab* mutants lacked SDP1, most peroxisomes appeared similar in size to *sdp1* mutants (Fig. 4d). However, a subpopulation of peroxisomes in *sdp1 pex11ab* mutants were large and lacked ILVs (Fig. 4d), perhaps because another TAG lipase, SDP1-like[63], remained present. The observation that pharmacological (Fig. 4b, c) or genetic (Fig. 4d) inhibition of lipid mobilization suppressed the large-peroxisome phenotype of *pex11ab* mutants indicates that TAG catabolism is necessary for the excessive *pex11ab* peroxisome enlargement and confirms that PEX11A/B restrains peroxisome expansion and promotes ILV formation during lipid mobilization. In contrast, the robust peroxisome expansion observed in *pex11cde*, even when lipid mobilization is impaired (Fig. 4b, c), reveals that PEX11C/D/E uses a different mechanism to limit peroxisome enlargement.

ILVs in wild-type seedlings appear to move freely within the peroxisome lumen, whereas subpopulations of enlarged peroxisomes in β-oxidation mutants sometimes contain ILVs that appear affixed to the outer membrane adjacent to lipid droplets[36]. Similarly, we observed a

https://doi.org/10.1038/s41467-026-71873-3

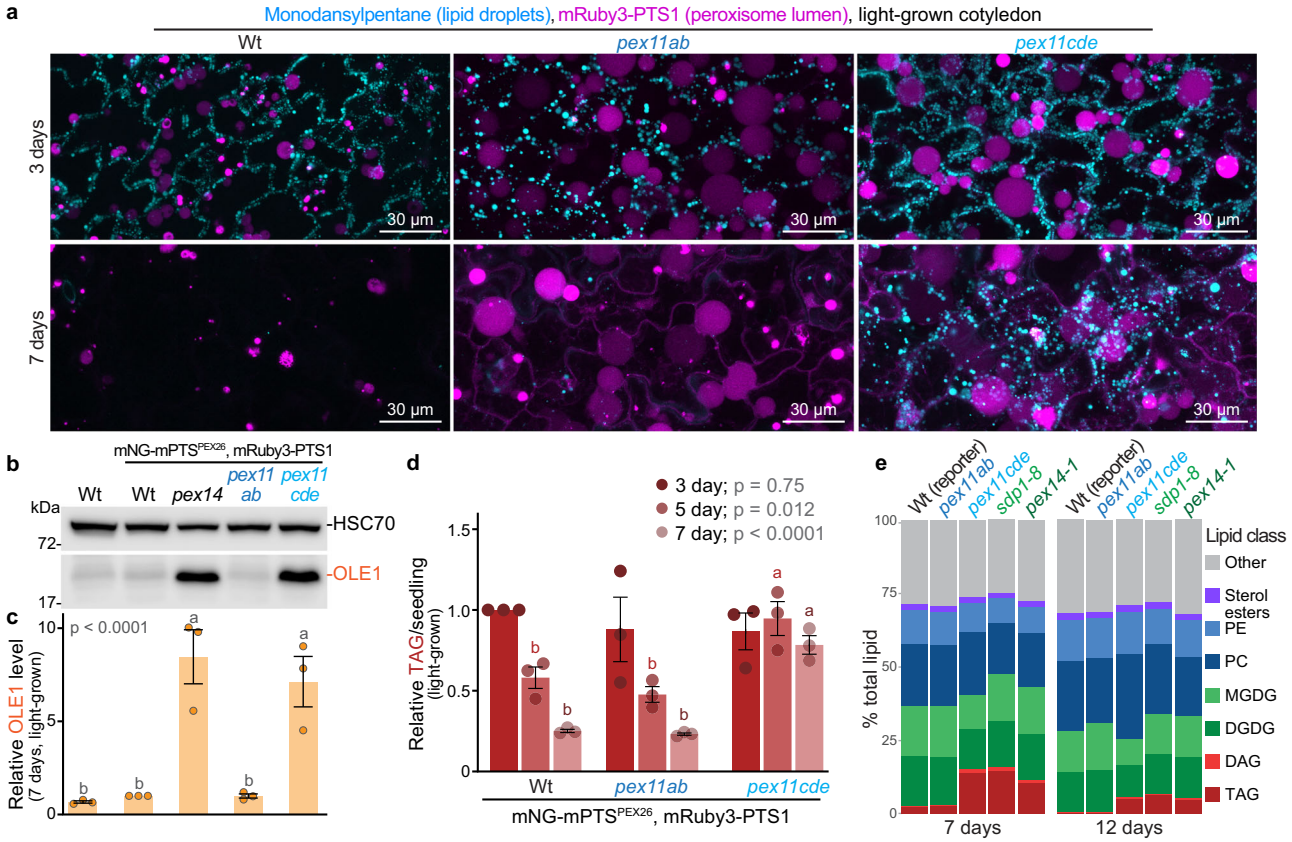

Fig. 3 | PEX11 isoforms differentially contribute to lipid metabolism. **a** Maximum-intensity projections [ten 1-µm (top) or 3-µm (bottom) steps] of the seedlings imaged in Fig. 1d showing peroxisomes (mRuby3-PTS1, magenta) and lipid droplets (cyan). At least five seedlings were imaged for each genotype and time point, and three images were used to quantify peroxisome size and number in Fig. 1. **b** Immunoblot of 7-day-old seedlings probed with antibodies recognizing HSC70 (loading control) or OLE1. The positions of molecular mass markers (in kDa) are shown on the left. **c** Relative OLE1 levels from three biological replicate immunoblots, including the one shown in **b**. Error bars represent SEM. **d** TAG levels during seedling development monitored via thin-layer chromatography. Bars represent mean TAG levels relative to the wild-type reporter line from three biological replicates (dots); error bars represent SEM. Letters above bars in **c** and **d** represent homologous subsets assigned by Tukey's post-hoc test when one-way ANOVA p-values were <0.05. In **d**, separate one-way ANOVA tests were performed to compare genotypes at each time point. **e** Relative contributions of major lipid classes to total lipid content in mutant seedlings and the wild-type reporter line. TAG, triacylglycerols; DAG, diacylglycerols; DGDG, digalactosyldiacylglycerols; MGDG, monogalactosyldiacylglycerols; PC, phosphatidylcholines; PE, phosphatidylethanolamines.

subpopulation of enlarged peroxisomes in older *ped1* mutant seedlings with ILVs sequestered to the peroxisome membrane adjacent to lipid droplets (Fig. 4e), consistent with the hypothesis that peroxisomal ILVs function in lipid mobilization[6,36]. Moreover, some peroxisomes in 7-day-old *ped1 pex11ab* mutants were enlarged and contained ILVs apposed to lipid droplets (Fig. 4e). The presence of ILVs in these expanded *ped1 pex11ab* peroxisomes supports our time-lapse data showing that PEX11A/B is not absolutely required for ILV formation (Fig. 1i, Supplementary Movie 1) and suggests that β-oxidation of ILV lipids might contribute to the apparent ILV deficit in *pex11ab* mutants.

Because peroxisome expansion in *pex11ab*, but not *pex11cde*, required active lipid mobilization (Fig. 4), we examined peroxisomes in tissues with different dependencies on β-oxidation. For example, "true" leaves form post-embryonically from the shoot apical meristem (Fig. 5a) and rely on photosynthesis rather than stored lipids for energy[64]. We found that *pex11ab* leaf peroxisomes resembled wild-type peroxisomes, whereas *pex11cde* leaf peroxisomes were enormous and lacked ILVs (Fig. 5b), supporting the conclusion that PEX11C/D/E restrains peroxisome enlargement independently of lipid mobilization.

The pattern of enlarged peroxisomes in *pex11* roots was also linked to lipid mobilization. Germinating seedling roots utilize lipid droplets deposited during embryogenesis, whereas roots in older plants rely on photosynthate from the shoot. In the root meristem, daughter cells arising from dividing stem cells are displaced as the root grows downward (Fig. 5a). Thus, the primary root provides a chronological record of root cell birth and differentiation[65], with the oldest root cells adjacent to the hypocotyl. *pex11ab* seedlings only displayed enlarged peroxisomes in mature root cells (Fig. 5c), which descended from embryonic root cells that were packed with lipid droplets. As in older cotyledon cells (Fig. 1d), these enlarged *pex11ab* mutant peroxisomes mostly lacked ILVs (Fig. 5c). In contrast, *pex11cde* mutants already contained larger peroxisomes than *pex11ab* or wild-type seedlings in the young cells of the root meristem (Fig. 5c). Most of these enlarged peroxisomes in *pex11cde* root meristem contained abundant ILVs, demonstrating that PEX11C/D/E is not essential for ILV formation in these cells. Similarly, in the young differentiation zone (Fig. 5a), where cells exit the elongation zone and begin to form root hairs[65], *pex11cde* peroxisomes were enlarged with some ILVs (Fig. 5c). In the mature differentiation zone, however, the large peroxisomes of *pex11cde* mutants contained intralumenal membranes that often appeared as stringy or clumped internal membranes rather than the usual spherical vesicular architecture in cells from younger root zones (Fig. 5c), suggesting that PEX11C/D/E is needed to correctly shape or maintain newly forming ILVs. The distinct peroxisome expansion defects observed in the corresponding *pex11* mutants suggest that PEX11A/B and PEX11C/D/E have different functions.

https://doi.org/10.1038/s41467-026-71873-3

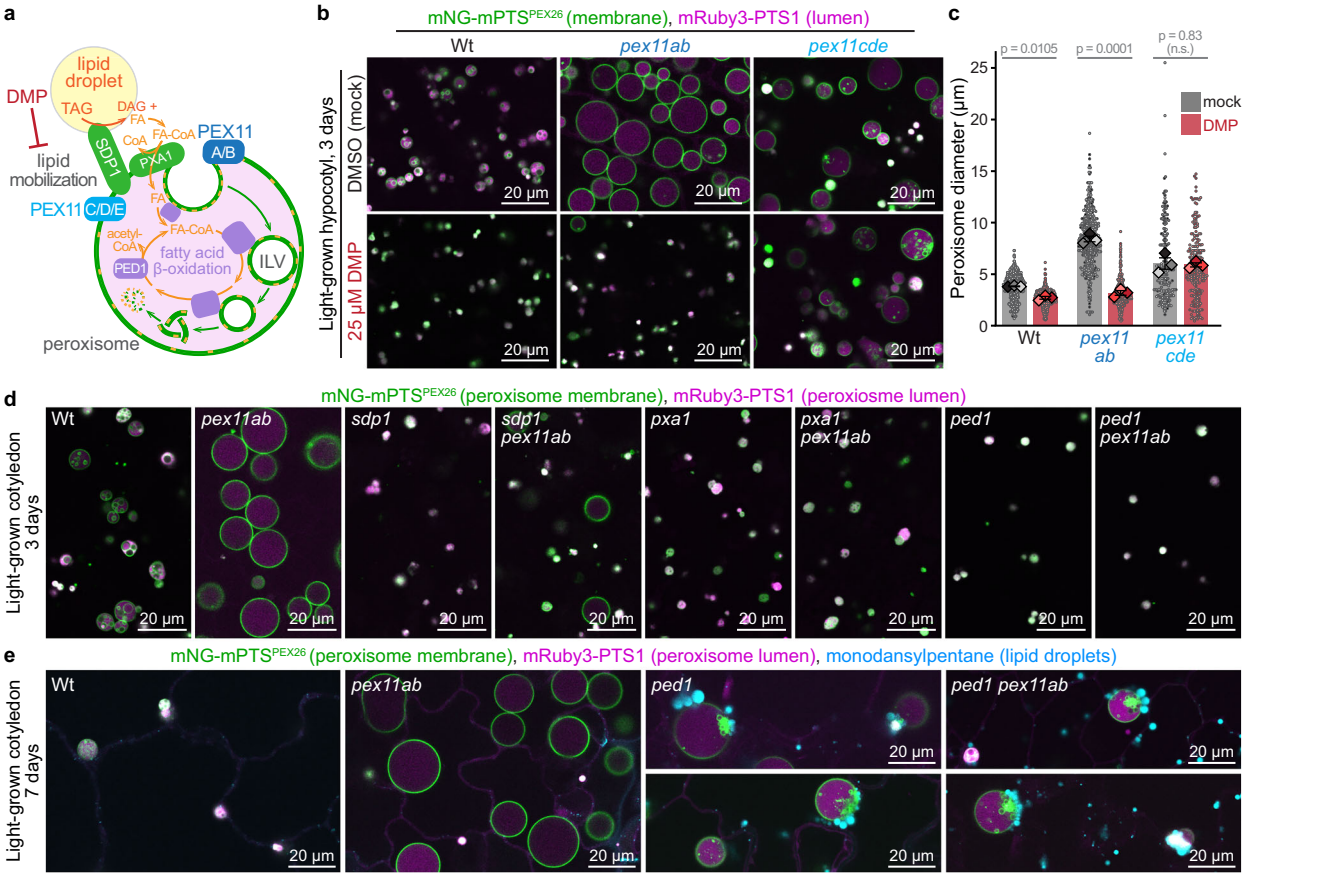

Fig. 4 | PEX11 isoforms play different roles in shaping peroxisome membranes during lipid mobilization. a Model of lipid droplet-peroxisome collaboration during lipid mobilization. SDP1 is a triacylglycerol (TAG) lipase, PXA1 is a fatty acid (FA) transporter, PED1 is a thiolase acting in β-oxidation, and diphenyl methylphosphonate (DMP) blocks lipid mobilization. **b** Confocal images of peroxisomes in seedlings expressing mNeonGreen-mPTS^{PEX26} (green) and mRuby3-PTS1 (magenta) grown without or with DMP to slow lipid mobilization. **c** Quantification of peroxisome size from **b**. Individual peroxisome diameters (dots) from three individual seedlings are shown in three shades of gray or red; bars represent means of the replicates (diamonds); error bars represent SEM. P-values from two-tailed Student's t-tests comparing the means of mock and treated conditions are shown. **d**, **e** Confocal images of peroxisomes in 3- (**d**) or 7-day-old (**e**) seedlings of the indicated genotypes expressing mNeonGreen-mPTS^{PEX26} (green) and mRuby3-PTS1 (magenta). Lipid droplets (cyan) were stained using monodansylpentane in **e**. In **d** and **e**, at least three seedlings were imaged for each genotype, and representative images are shown.

PEX11A/B and PEX11C/D/E support ILV formation and restrain peroxisome size via distinct mechanisms

Because varying expression could contribute to different *pex11* mutant phenotypes, we examined *PEX11* transcript levels in an RNA-seq atlas[66]. All five *PEX11* isoforms were expressed during seed germination, with *PEX11D* and *E* transcripts more abundant than *PEX11A*, *B*, or *C* transcripts (Supplementary Fig. 7). Additionally, *PEX11A*, *C*, and *E* transcripts were present at similar levels in 1-day-old seedling roots, whereas *PEX11D* transcripts were low in roots but more abundant in cotyledons and hypocotyls than the other transcripts (Supplementary Fig. 7).

The observation of dramatically enlarged peroxisomes in *pex11ab* mutant cotyledons (Fig. 1) despite abundant *PEX11D* transcripts in cotyledons (Supplementary Fig. 7d) suggested that the differences observed in *pex11ab* and *pex11cde* mutants originated from functional differences among the corresponding proteins. To test this possibility, we expressed mTagBFP2-tagged versions of PEX11B or PEX11E (Fig. 6a) from an estradiol-inducible promoter[67] in *pex11ab* and *pex11cde* mutants. Immunoblotting following growth on estradiol revealed that mTagBFP2-HA-PEX11E accumulated to higher levels than mTagBFP2-HA-PEX11B in the selected transgenic lines (Fig. 6b).

As expected from prior studies showing tagged Arabidopsis PEX11 isoforms at peroxisomal membranes[23,27], both mTagBFP2-HA-PEX11B and mTagBFP2-HA-PEX11E co-localized with the mNeonGreen-mPTS^{PEX26} peroxisomal membrane marker (Fig. 6c, d, Supplementary Fig. 8). We found that the subset of *pex11ab* cells that accumulated mTagBFP2-PEX11B following estradiol induction showed restored peroxisome size and ILV formation, whereas adjacent cells without mTagBFP2-HA-PEX11B still contained large peroxisomes lacking ILVs (Fig. 6c). In contrast, expression of mTagBFP2-HA-PEX11E in *pex11ab* seedlings did not restore ILV content. Instead, peroxisomes in seedlings that appeared to have lower mTagBFP2-HA-PEX11E levels were ringed with mTagBFP2-HA-PEX11E, but largely lacked ILVs, like the original *pex11ab* mutant (Fig. 6c, fourth column). Even seedlings with higher mTagBFP2-HA-PEX11E accumulation, which contained smaller, clustered, and occasionally elongated (tubulated) peroxisomes (or peroxules), often lacked peroxisomal ILVs (Fig. 6c, sixth column, Supplementary Movie 2). The ability of the PEX11E reporter to decrease peroxisome size in *pex11ab* without restoring peroxisomal ILV content indicates that PEX11A/B has a role in ILV formation that cannot be performed by PEX11E. Intriguingly, expressing yeast Pex11 (mTagBFP2-HA-ScPex11) complemented *pex11ab* peroxisome size and ILV defects (Fig. 6e), suggesting conserved PEX11 function in other eukaryotes.

In reciprocal experiments, expression of mTagBFP2-HA-PEX11E clearly restored *pex11cde* peroxisome size to resemble wild type, whereas *pex11cde* cells accumulating mTagBFP2-HA-PEX11B did not

https://doi.org/10.1038/s41467-026-71873-3

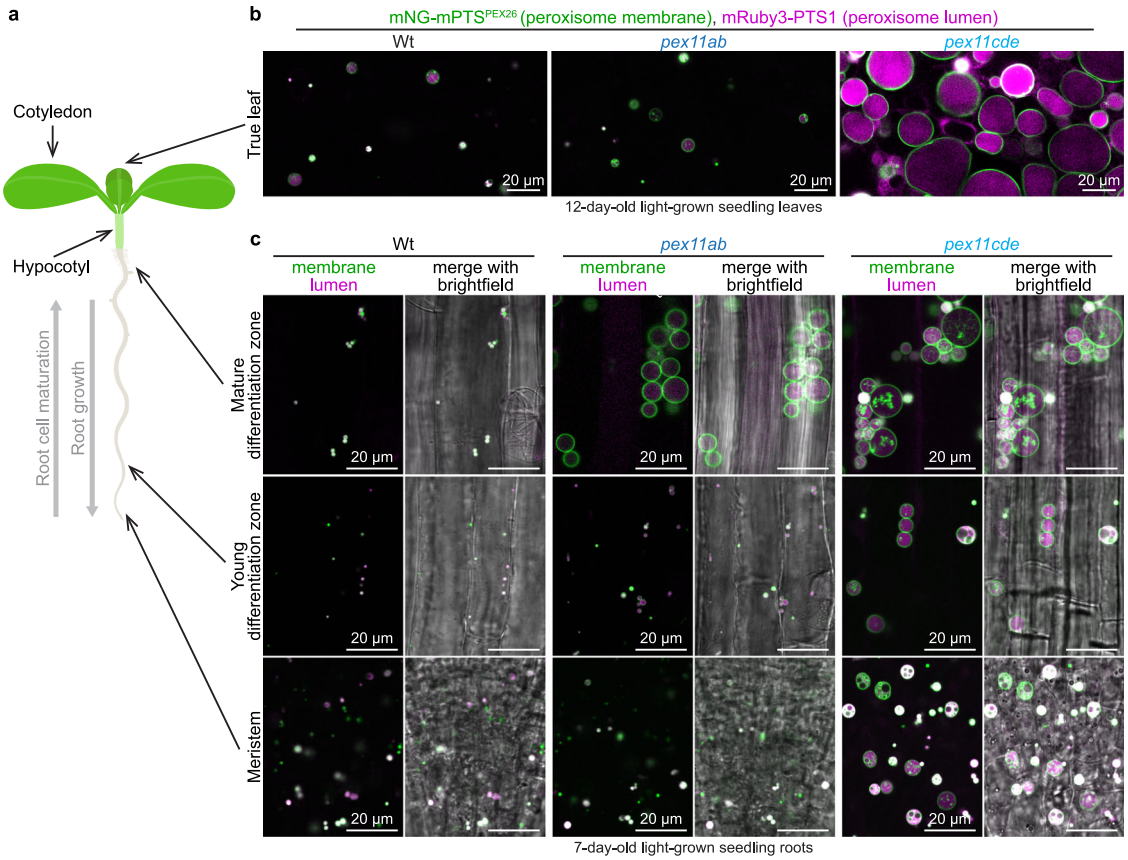

Fig. 5 | *PEX11* genes differentially control peroxisome size and ILV formation in true leaves and roots. a Seedling diagram indicating tissues imaged. **b** Confocal images of leaf peroxisomes in 12-day-old seedlings. At least three seedlings were imaged for each genotype, and representative images are shown. **c** Confocal images of root peroxisomes in 7-day-old seedlings. At least four seedlings were imaged for each genotype and tissue, and representative images are shown.

display appreciably altered peroxisomes compared to neighboring cells that did not accumulate the reporter (Fig. 6d). Together, these complementation experiments demonstrate that the peroxisome morphology defects observed in the *pex11* mutants stemmed from deficiencies in the corresponding *PEX11* genes, that the N-terminal tag did not notably interfere with PEX11 function in regulating peroxisome size, and that PEX11A/B and PEX11C/D/E play distinct roles in sculpting peroxisomal membranes.

PEX11 is essential for seedling survival in Arabidopsis

To determine if PEX11C/D/E also perform redundant roles with PEX11A/B in peroxisome biology, we sought higher-order *pex11* mutants. We used our three-gRNA CRISPR system to target *PEX11C-E* in a *pex11ab* mutant and identified several viable quadruple mutants (Supplementary Table 1, 2). Growth of *pex11abcd* quadruple mutant seedlings was similar to *pex11ab* mutants, with a slight defect when grown without sucrose, whereas *pex11abce* mutants had a moderate growth defect and some sucrose dependence but were less impaired than the *pex11cde* mutant (Supplementary Fig. 3a). Genotyping the adult progeny of a homozygous *pex11abcd* mutant that was also heterozygous for a *pex11e* mutation did not reveal any homozygous *pex11abcde* quintuple mutants, indicating that the absence of all PEX11 isoforms conferred embryonic or seedling lethality. We did not observe shriveled or missing seeds in seedpods from *pex11* hemiquintuple (*pex11a/a b/b c/c d/d E/e*) mutants, suggesting that, unlike many peroxin null alleles[68–73], the quintuple *pex11* mutant did not display embryonic or gametophytic lethality. Indeed, when we genotyped seedlings from a *pex11* hemiquintuple parent, we found *pex11abcde* seedlings at the expected Mendelian ratio (~25%; Fig. 7b). However, the tiny *pex11abcde* quintuple mutant seedlings were even smaller than *pex11cde* mutants on sucrose-supplemented medium (Fig. 7a) and did not survive after transfer to soil, indicating that PEX11C/D/E and PEX11A/B functions are together essential for plant survival.

Like *pex11abcd* and *pex11cde* mutants, *pex11abcde* mutants contained large peroxisomes with sparse ILVs compared to wild type (Fig. 7c, d). Occasionally, the massively enlarged peroxisomes in *pex11abcde* mutants appeared to compromise the final cell division needed for stomate formation. Guard cells and pavement cells arise from post-embryonic cell divisions from the same meristemoid precursors[74], and the two guard cells that form a stomate are small compared to the pavement cells that comprise most of the epidermis. The extreme peroxisome enlargement in the *pex11abcde* mutant sometimes resulted in normally spherical peroxisomes becoming elongated due to the limits imposed by the guard cell walls (Fig. 7c). In some instances, these elongated *pex11abcde* peroxisomes were positioned perpendicularly to the stomatal opening and appeared to have occluded the final symmetrical cell division that produces two guard cells from a guard mother cell (Fig. 7c, last column). The presence of constrained peroxisomes in deformed stomata suggests that the PEX11 family prevents peroxisomes from occupying an excessive volume, thereby allowing cell division.

Surprisingly, peroxisomes remained even more abundant in *pex11abcde* than in wild-type seedlings (Fig. 7d, e), conclusively demonstrating that PEX11 is not essential for peroxisome proliferation in Arabidopsis cotyledons. The enhanced defects of *pex11abcde* mutants imply that both PEX11 clades cooperatively regulate peroxisome size and morphology.

https://doi.org/10.1038/s41467-026-71873-3

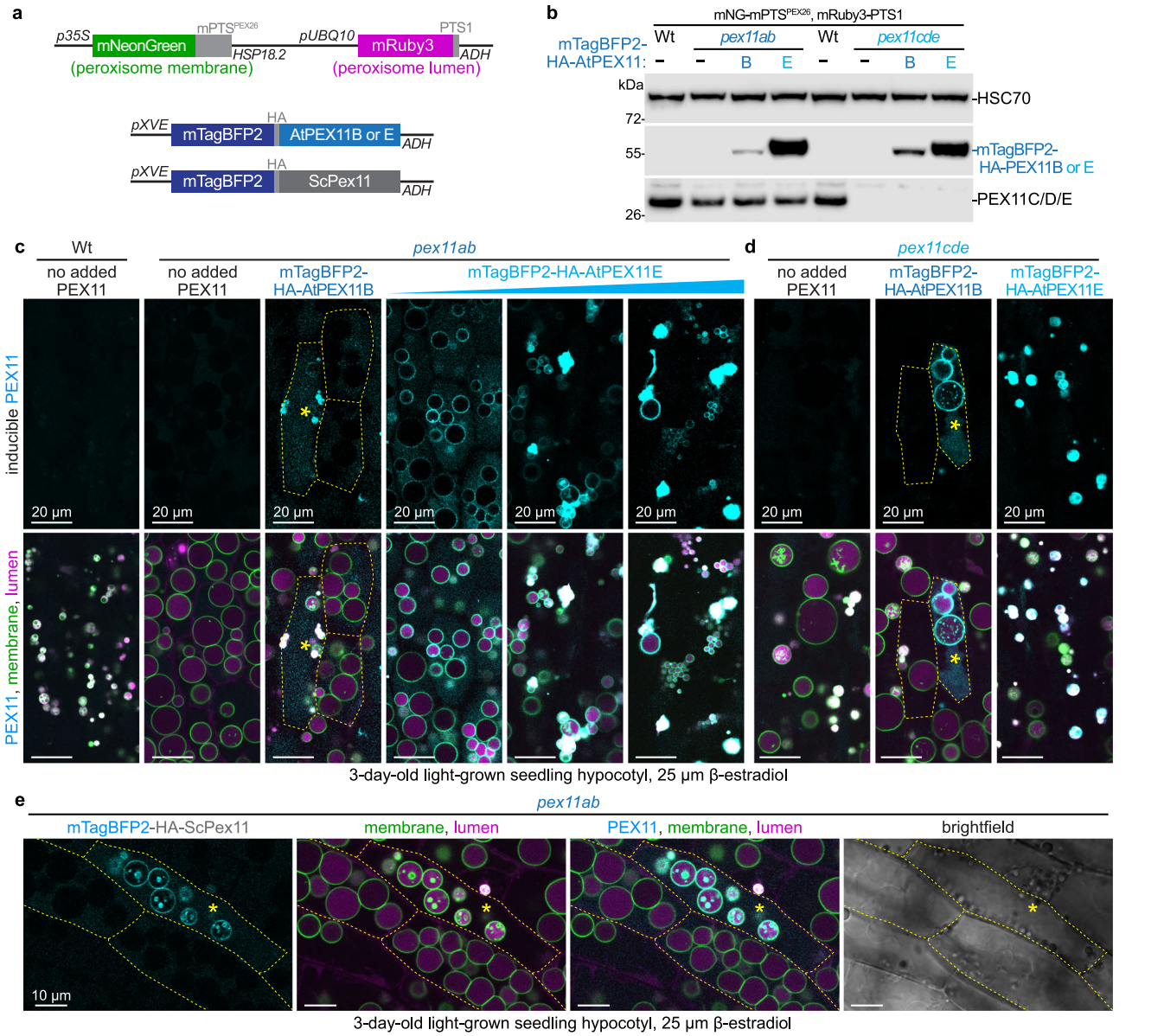

Fig. 6 | PEX11 isoforms have distinct functions. a Constructs expressing mTagBFP2-HA-PEX11 from the β-estradiol-inducible *pXVE* promotor were introduced into *pex11* mutants carrying the mNeonGreen-mPTS^{PEX26} and the mRuby3-PTS1 peroxisome reporters. **b** Immunoblot monitoring mTagBFP2-HA-PEX11 accumulation (detected with an anti-HA antibody) in 3-day-old light-grown seedlings grown on 25 µM β-estradiol. HSC70 is a loading control, and an anti-PEX11E antibody was used to detect PEX11C/D/E in a single experiment, assessed in two technical replicates. **c**, **d** Confocal images of peroxisomes in wild-type, *pex11ab*, and *pex11ab* expressing the indicated mTagBFP2-HA-AtPEX11 reporter (**c**) or *pex11cde* and *pex11cde* expressing the indicated mTagBFP2-HA-AtPEX11 reporter (**d**) after growth on β-estradiol. Brightfield channels (Supplementary Fig. 8) were used to visualize individual hypocotyl cell borders (dashed lines); asterisks indicate outlined cells with detectable mTagBFP2-HA-AtPEX11B fluorescence. Images of *pex11ab* seedlings with increasing levels of mTagBFP2-HA-PEX11E are shown in **c** (blue triangle). **e** Confocal images of peroxisomes in *pex11ab* expressing mTagBFP2-HA-ScPex11. The brightfield channel was used to visualize individual hypocotyl cell borders (dashed lines); an asterisk marks a cell with detectable mTagBFP2-HA-ScPex11 fluorescence. In **c**–**e**, at least four (**c**), three (**d**), or eight (**e**) seedlings were imaged for each genotype, and representative images are shown.

Discussion

By generating *pex11* null mutants in Arabidopsis, we confirmed a role for PEX11 in limiting peroxisome size and discovered that peroxisomal ILV abundance is dependent on PEX11. Among the five Arabidopsis PEX11 isoforms, PEX11A/B limits peroxisome size during the lipid mobilization that drives early seedling growth, whereas PEX11C/D/E is essential for normal lipid metabolism and plant growth, and limits peroxisome size in diverse tissues even in the absence of lipid mobilization (Fig. 7f). Together, these distinct PEX11 functions in maintaining peroxisome size and morphology are essential for plant life.

PEX11 is typically thought to initiate peroxisome division. However, the dramatically increased peroxisome size in *pex11ab* mutants was not accompanied by similarly decreased peroxisome abundance (Fig. 1), which would follow division defects. Furthermore, inhibiting lipid mobilization prevented *pex11ab* (and wild-type) peroxisome enlargement (Fig. 4), indicating that this enlargement required fatty acids from lipid droplets. Similarly, yeast *pex11* mutant peroxisomes are small unless grown on oleate-containing media[19], and yeast Pex11 is implicated in fatty acid import[75]. Our observation that yeast Pex11 can restore ILV content and peroxisome size in the Arabidopsis *pex11ab* mutant (Fig. 6e) hints that the connections between PEX11, peroxisome

https://doi.org/10.1038/s41467-026-71873-3

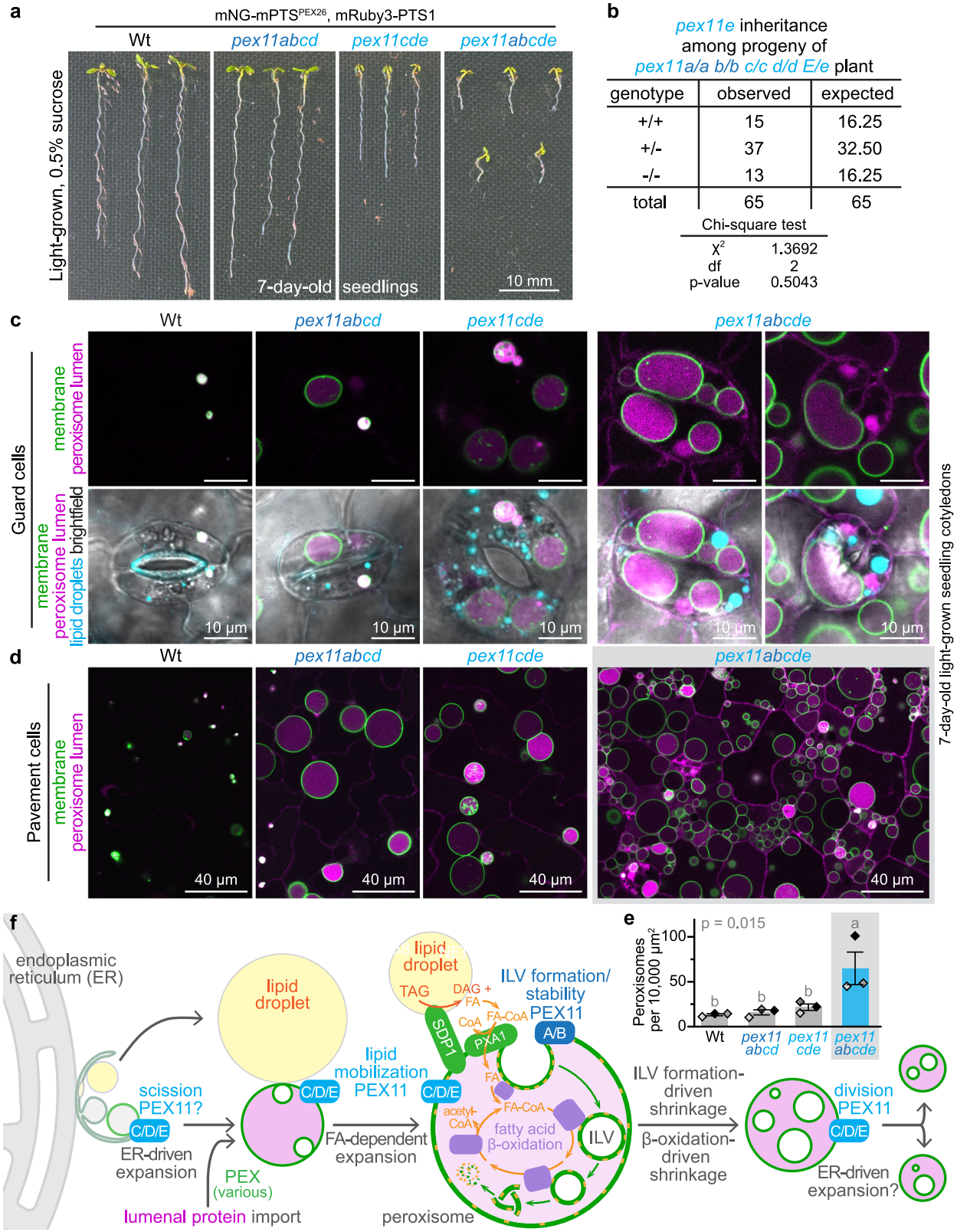

Fig. 7 | PEX11 is essential for seedling development and peroxisome function. **a** Photograph of seedlings. **b** *PEX11E* inheritance among the seedling progeny of a *pex11a/a b/b c/c d/d E/e* mutant plant. Chi-square analysis with Pearson's test was used to show that the *pex11a/a b/b c/c d/d e/e* mutations did not confer embryonic lethality. **c**, **d** Confocal images of epidermal guard cells (**c**) or pavement cells (**d**) of seedlings expressing mNeonGreen-mPTS^{PEX26} (green) and mRuby3-PTS1 (magenta). Lipid droplets (cyan) were stained using monodansylpentane in **c**. **e** Quantification of peroxisome abundance. Bars show the mean number of peroxisomes from three seedling cotyledon images (diamonds) for each genotype; error bars represent SEM. Letters above bars represent homologous subsets from Tukey's post-hoc test following one-way ANOVA. The lack of shared letters indicates a significant difference between the means. **f** Model depicting potential PEX11 roles (blue) in ER-driven peroxisome expansion, lipid droplet-peroxisome collaboration during fatty acid (FA) β-oxidation, intralumenal vesicle (ILV) formation, and peroxisome division.

size, and lipid mobilization observed in other systems[16,19,21,22] may, at least in part, reflect peroxisomal ILV formation during lipid mobilization (Fig. 7f).

Catabolism of the fatty acids liberated from TAG at lipid droplet-peroxisome contact sites requires membrane-localized transporters to import fatty acids into peroxisomes[76,77]. Because long-chain fatty acids are virtually insoluble in water[78], it is unlikely that these fatty acids would be imported like water-soluble metabolites. Instead, long-chain fatty acids might insert into the peroxisomal membrane and become accessible to the lumen through peroxisomal fatty-acid transporters acting to flip fatty acids to the inner leaflet of the lipid bilayer[76]. ILVs could then assist lipid import by bringing membranes laden with free fatty acids or fatty acyl-CoAs into the peroxisome lumen (Fig. 7f). Indeed, peroxisome membranes in young cotton seedlings contain abundant free fatty acids derived from lipid droplet TAG[79]. Moreover, ESCRT disruptions impair not only peroxisomal ILV formation but also lipid mobilization, and β-oxidation enzyme mutants display ILV defects (Fig. 4e)[36]. Although the composition of ILV membranes is unknown, our data support the idea that peroxisomal ILV membranes might harbor lipids from lipid droplets.

The propensity of long-chain fatty acids or fatty acyl-CoAs to permeabilize and destabilize membranes[80] would presumably limit the concentration of free fatty acids in ILV membranes. Perhaps some TAG-derived lipids are converted into phospholipids and delivered to the peroxisome membrane to fuel ILV formation, rather than being immediately hydrolyzed to free fatty acids. This idea is supported by the observation that cotton seedling peroxisomes contain phospholipids derived from lipid droplet TAG[79]. Phospholipids incorporated into the peroxisome bilayer could enter peroxisomes via ILV invagination, be degraded by intraperoxisomal phospholipases, and finally catabolized through β-oxidation. Drosophila *pex2* and *pex16* mutants accumulate phospholipid precursors and are deficient in phospholipid degradation products[81]. Similarly, 12-day-old *pex11cde* mutant seedlings had increased PC levels (Fig. 3e, Supplementary Fig. 6), hinting that phospholipid degradation may be a normal peroxisomal process. This model would explain why a yeast peroxisomal phospholipase mutant displays peroxisomal ILVs[82] and defects in β-oxidation[83], and why an Arabidopsis peroxisomal β-oxidation enzyme mutant appears to accumulate peroxisomal ILVs (Fig. 4e)[52].

Given these connections between lipid mobilization, peroxisome enlargement, and ILV formation, it was curious that the notable *pex11ab* peroxisomal ILV defects (Fig. 1) were not accompanied by the severe physiological defects that are hallmarks of impaired β-oxidation (Fig. 2). However, unlike *pex11cde* mutants, and like wild-type peroxisomes, *pex11ab* peroxisomes shrank and acquired internal membranes as seedlings developed (Fig. 1), indicating that ILV formation is only partially disrupted in the absence of PEX11A/B. Moreover, genetically impairing β-oxidation by introducing a *ped1* mutation into the *pex11ab* mutant revealed ILVs adjacent to lipid droplets in enlarged peroxisomes (Fig. 4e), again demonstrating that ILVs can form without PEX11A/B and suggesting that these ILVs are broken down by the PED1 thiolase. Perhaps, without PEX11A/B, inefficient ILV formation during lipid mobilization results in excessive peroxisome enlargement, while the continued degradation of the ILVs that do form allows fat utilization and seedling growth.

Unlike *pex11ab*, very young *pex11cde* tissues contained fewer peroxisomes than wild type (Fig. 1g, Supplementary Fig. 4c), consistent with a role for PEX11C/D/E in peroxisome proliferation. Moreover, expressing mTagBFP2-HA-PEX11E in the *pex11ab* mutant resulted in numerous small peroxisomes (Fig. 6c), indicating that PEX11E can increase peroxisome abundance. We also detected tubulated membranes in *pex11ab* cells with higher mTagBFP2-HA-PEX11E accumulation, consistent with prior studies demonstrating that PEX11 overexpression can induce peroxisome tubulation, which has been hypothesized to precede division[13,23,24,26,27]. However, the striking peroxisome expansion in older *pex11cde* mutant cotyledons was not accompanied by decreased peroxisome numbers, and reduced peroxisome fission cannot completely account for the dramatic increase in total peroxisome volume in this tissue (Fig. 1, Supplementary Fig. 2f). We conclude that PEX11C/D/E, like PEX11A/B, has roles beyond peroxisome division, which might include regulation of pexophagy[84,85] and/or biogenesis from the ER[6,29,86,87] (Fig. 7f).

Like in *pex11ab* mutants, the enlarged peroxisomes in *pex11cde* mutants often appeared to lack ILVs (Fig. 1c). The enlarged *pex11cde* peroxisomes, even in tissues where β-oxidation is not particularly active (e.g., true leaves (Fig. 5b) and young root cells (Fig. 5c)), suggest a role for peroxisomal ILVs beyond lipid mobilization. Indeed, blocking lipid droplet mobilization did not prevent the excessive enlargement of *pex11cde* peroxisomes (Fig. 4b, c). Perhaps peroxisome enlargement in *pex11cde* mutants derives from increased phospholipid transfer from a non-lipid droplet source. For example, non-vesicular lipid transfer from the ER supports the expansion of multiple compartments[88,89], including peroxisomes[6,90–92], and might supply *pex11cde* peroxisomes with excess lipids. Alternatively, a failure of newly synthesized peroxisomes to efficiently detach from the ER might contribute to excessive peroxisome expansion in *pex11cde* (Fig. 7f). Either hypothesis could explain the increased PC levels in *pex11cde* (Fig. 3e, Supplementary Fig. 6).

pex11cde seedlings, unlike *pex11ab*, inefficiently mobilized lipid droplets, leading to TAG retention and sucrose-dependent seedling growth (Figs. 2, 3, Supplementary Fig. 6). Lipid droplet TAG is hydrolyzed by the peroxisomal membrane lipase SDP1[55] to form DAG and a free fatty acid, which is transported into the peroxisome via PXA1[61] for β-oxidation (Fig. 4a). PEX11E interacts with FREE1[44], an early-acting plant-specific ESCRT protein[93], which might initiate the ESCRT cascade to form peroxisomal ILVs. Intriguingly, FREE1 also interacts with SDP1[44]. Perhaps PEX11C/D/E binding to FREE1 promotes FREE1-SDP1 interactions to assist the lipid droplet–peroxisome contacts that facilitate lipid mobilization in addition to initiating the ESCRT cascade that forms peroxisomal ILVs.

In addition to bringing effector proteins to the peroxisome, PEX11 may have intrinsic properties that contribute to *pex11* mutant phenotypes. For example, predicted Arabidopsis PEX11 structures reveal a small channel through the six predicted alpha-helices (Supplemental Fig. 1c), and yeast Pex11 acts as a non-selective channel that transfers small solutes in vitro[75]. Intriguingly, a nonselective cation channel on the lysosome membrane, TMEM63A, allows lysosomal membrane deformation by releasing cationic osmoticants when lysosome membranes experience mechanical tension caused by increased turgor pressure[94]. If an osmoticant normally released by PEX11 builds up within the organelle, perhaps *pex11* mutant peroxisomes experience heightened turgor pressure, which impedes the membrane deformation that would allow ILV formation or peroxisome division. It will be interesting to learn whether Arabidopsis PEX11 acts as an ion channel, which solute(s) it transports, and whether PEX11 isoforms have different specificities.

Interestingly, *pex11cde* mutants displayed PTS2-processing defects (Fig. 2a, b), suggesting a direct or indirect role for PEX11C/D/E, and perhaps ILVs, in lumenal protein import. Indeed, a potential import role for ILVs was hypothesized when peroxisomes were originally found to import oligomeric proteins[37]. Perhaps ILV invagination assists canonical peroxisomal import[12] by sequestering cargo that is too large to import efficiently, potentially explaining the presence of PTS-containing proteins in a subset of ILVs[36]. The IBA resistance and plant growth defects observed in *pex11cde* mutants (Fig. 2, Supplementary Fig. 3) could stem from defects in lumenal protein import and/or the inefficiencies that could result from dramatically expanding the volume of the peroxisome lumen (Fig. 1h, Supplementary Fig. 2f). For example, the activity of DEG15, the enzyme responsible for cleaving PTS2-containing proteins[48–50], could be reduced in the diluted lumen of expanded peroxisomes.

In addition to the distinct functions of Arabidopsis PEX11A/B and C/D/E, the seedling lethality of the *pex11* quintuple mutant (Fig. 7a, b) could reflect overlapping functions or an essential role of cross-clade oligomers. All Arabidopsis PEX11 isoforms interact with each other[16], and PEX11 hetero-oligomers could mediate additional protein interactions and functions. *pex11* quintuple mutant peroxisomes in 7-day-old cotyledons were enlarged and devoid of ILVs (Fig. 7c, d), reinforcing the critical role for PEX11 in ILV formation. Remarkably, *pex11* quintuple mutants contained even more peroxisomes than wild type (Fig. 7d, e), indicating that Arabidopsis PEX11 is not essential for building peroxisomes. Moreover, the cellular crowding that ensues upon excessive peroxisome expansion could disrupt the functions of other organelles and cellular processes, including cell division (Fig. 7c). Beyond roles in development, plant *PEX11* genes are differentially induced upon biotic and abiotic stresses[46,95,96], and it will be interesting to learn the roles of PEX11 isoforms and peroxisomal ILVs under various stress conditions.

Other examined eukaryotes also have multiple PEX11 isoforms[10], and the distinctions between Arabidopsis PEX11 clade functions prompt the question of whether PEX11 isoforms function similarly in other species. The small size of peroxisomes in many organisms makes it nearly impossible to resolve sub-peroxisomal structures using light microscopy, and employing *pex11* mutants to allow imaging of larger peroxisomes[83] would fail to reveal ILVs if the ILV-promoting function of PEX11 is conserved. Prior studies have shown partial complementation of yeast *pex11* growth defects by some Arabidopsis PEX11 isoforms[23,97]. Yeast Pex11 is more closely related to Arabidopsis PEX11A/B than PEX11C/D/E[10], and we found that mTagBFP2-HA-ScPex11 complemented Arabidopsis *pex11ab* peroxisome size and ILV defects (Fig. 6e) hinting that the enlarged peroxisomes observed in yeast *pex11* mutants[19] could stem from impaired ILV formation. It will be interesting to learn if PEX11-dependent peroxisomal ILV formation is conserved in other organisms that display large peroxisomes upon PEX11 dysfunction.

In summary, we employed live-cell microscopy to demonstrate that Arabidopsis PEX11 isoforms differentially sculpt peroxisomal membranes to regulate organellar function. The PEX11 roles in ILV formation illuminated here may provide insight into PEX11 functions in other systems, including the pathophysiology of human PEX11 deficiencies[98–102], and inform future studies uncovering additional functions of internalized peroxisomal membranes.

Methods

Plant growth conditions and physiological assays

All plant lines were in the Columbia-0 accession of *Arabidopsis thaliana*. *pex14-1*[47] and the dual fluorescent reporter line marking peroxisome lumen (mRuby3-PTS1) and membrane (mNeonGreen-mPTS^{PEX26})[36] were described previously. *sdp1-8* (SALK_201353C) was generated by the Salk Institute Genomic Analysis Laboratory[103] and obtained from the Arabidopsis Biological Resource Center at The Ohio State University.

Plants were grown under continuous white light at 22 °C unless otherwise indicated. Seeds were surface sterilized and stratified for 1-3 days in 0.1% agar in the dark at 4 °C. Seeds were sown on plant nutrient (PN) media[104] supplemented with 0.5% sucrose (PNS). Media was solidified using 0.6% or 1% agar when growing seedlings horizontally or vertically, respectively. After 7-12 days, seedlings were transplanted to soil for seed production.

For light-grown sucrose dependence and IBA assays, seeds were sown on PNS supplemented with 10 µM IBA (from a 100 mM stock dissolved in ethanol), or PN or PNS supplemented with the same amount of ethanol, and grown vertically under continuous yellow-filtered light[105] for 7 days. For dark-grown sucrose dependence and IBA assays, seeds were germinated under continuous white light for 1 day. Seeds were then plated on PNS supplemented with 30 µM IBA, or PN or PNS supplemented with the same amount of ethanol, and incubated for 1 day under yellow-filtered light before plates were wrapped in foil and placed vertically for 4 days. Plates were scanned using a flatbed scanner, and seedling hypocotyls (dark-grown assays) or roots (light-grown assays) were measured using ImageJ/FIJI (version 1.54p). Seedlings that did not germinate were not measured, except in Supplementary Fig. 3a, where seedlings that did not germinate were quantified as 0.

For lateral root assays, seedlings were grown vertically on PNS under continuous white light for 4 days before being transferred to PNS supplemented with 8 µM IBA, or PNS supplemented with the same amount of ethanol, and grown under yellow-filtered light for an additional 4 days, after which lateral roots that had emerged from the primary root were counted using a dissecting microscope, and the primary root length was measured to the nearest 1 mm using a ruler.

Seedlings and adult plants were photographed using an Apple iPhone camera. Image brightness was corrected using Adobe Photoshop (version 26.11). Representative 7-day-old seedlings grown on PN or PNS were transferred to a fresh plate and photographed. For *pex11* quintuple mutant seedlings, 7-day-old PNS-grown seedlings from a *pex11a/a b/b c/c d/d E/e* parent were photographed, and homozygous quintuple mutants were identified via genotyping. For adult plant analyses, 8-day-old seedlings were transplanted from PNS to soil, and plant survival was monitored twice a week over 35 days. Rosettes were photographed at 25 days. To measure rosette diameter, a circle encompassing the rosette was drawn using FIJI, and Microsoft Excel (version 2508) was used to calculate the diameter from the circumference.

Computational methods

Arabidopsis PEX11 protein sequence alignment, phylogenetic cladogram, and percent identity matrix were generated using MegAlign (DNAStar version 10.0.1). The sequence alignment was performed using the ClustalW method (BLOSUM series protein weight matrix). The AlphaFold Protein Structure Database (https://alphafold.ebi.ac.uk/)[106,107] was used to generate structural predictions. The TmAlphaFold Transmembrane Protein Structure database (https://tmalphafold.ttk.hu/)[108] was used to predict transmembrane domains and the position of PEX11 in the membrane. ENDscript 2.0 (https://endscript.ibcp.fr/ESPript/ENDscript/)[109] was used to delineate secondary structure elements. ChimeraX (version 1.10.1)[110,111] was used to render PEX11 structures and determine root mean square deviation (RMSD) scores with the Matchmaker function using the Needleman-Wunsch alignment algorithm and the BLOSUM-62 similarity matrix.

DNA methods

The CRISPR-Cas9-gRNA constructs were generated in the pAGM55261 vector[45]. The CHOPCHOP application (https://chopchop.cbu.uib.no/)[112] was used to identify sgRNA targets in the coding region of Arabidopsis *PEX11A-E*, *SDP1*, *PXA1*, and *PED1* genes (Supplementary Table 3). To target single genes (*SDP1*, *PXA1*, and *PED1*), complementary gRNA oligos with BsaI handles were annealed. To target multiple PEX11 genes, GenScript synthesized constructs containing tandem PEX11A/B and PEX11C/D/E gRNAs flanked by BsaI cut sites. To generate CRISPR-Cas9 constructs, annealed sgRNA oligos or synthesized plasmids were cloned into BsaI sites of the pAGM55261 vector (Addgene 153210)[45] using Golden Gate assembly (New England Biolabs, E1601) to yield Cas9-expressing vectors with gRNA sequences flanked by a U6 promoter and gRNA scaffold.

Constructs containing mTagBFP2-HA-AtPEX11B or mTagBFP2-HA-AtPEX11E were generated from a p35S-mTagBFP2-HA, pACT2-tdTomato-PTS1, pUBQ10-mNeonGreen-mPTS^{PEX26} trifluorescent construct in pUC57[6]. The full-length *AtPEX11B* (At3g47430) and *AtPEX11E* (At3g61070) genes (exons and introns) were PCR amplified using Q5 high-fidelity DNA polymerase (New England Biolabs, M0491) and

Gibson assembly primers (Supplementary Table 4) from *A. thaliana* genomic DNA and cloned into the NcoI site (downstream of the HA tag) of the trifluorescent construct via Gibson assembly (New England Biolabs, E2611). The resultant plasmids were digested with XhoI and religated with Quick Ligase (New England Biolabs, M2200) to remove 35S promoter and then digested with AvrII and NheI and religated to remove pACT2-tdTomato-PTS1 and pUBQ10-mNeonGreen-mPTS^{PEX26}. To generate mTagBFP2-HA-ScPEX11, *ScPEX11* (YOL147C) was PCR amplified from W303 *S. cerevisiae* genomic DNA using Gibson assembly primers (Supplementary Table 4) and cloned into mTagBFP2-HA-AtPEX11E cut with NcoI (to remove *AtPEX11E*) using Gibson assembly. The mTagBFP2-HA-PEX11 entry vectors were recombined into the pFZ19[67] plasmid using LR Clonase II (Invitrogen, 11791-020) to generate plant transformation vectors designed to inducibly express PEX11 variants using β-estradiol.

Plasmids were verified by sequencing via assembled Oxford Nanopore reads by Plasmidsaurus (Eugene, OR).

Arabidopsis transformation

Constructs were transformed into *Agrobacterium tumefaciens* GV3101 (containing the pMP90 plasmid)[113] by electroporation. Plants were transformed using a modified version of the floral dip method[114]. To generate *pex11* clade mutants, Agrobacterium strains containing CRISPR-Cas9 constructs targeting *PEX11A/B* or *PEX11C/D/E* were used to transform plants expressing mRuby3-PTS1 and mNeonGreen-mPTS^{PEX26} reporters[36]. To generate *sdp1*, *pxa1*, and *ped1* mutations, Agrobacterium strains containing CRISPR-Cas9 constructs targeting *SDP1*, *PXA1*, or *PED1* were used to transform wild-type and *pex11ab* mutants expressing the mRuby3-PTS1 and mNeonGreen-mPTS^{PEX26} reporters. To generate *pex11* quintuple mutants, *pex11ab* mutants were transformed with an Agrobacterium strain containing a CRISPR-Cas9 construct targeting *PEX11C/D/E*.

For complementation experiments, the *pex11ab* mutant was transformed with Agrobacterium strains containing constructs for expressing mTagBFP2-HA-AtPEX11B, mTagBFP2-HA-AtPEX11E, or mTagBFP2-HA-ScPex11. Transformants carrying mTagBFP2-HA-PEX11 constructs were selected by either hygromycin resistance or estradiol-inducible mTagBFP2 expression. The *pex11cde* mutant was transformed directly with the Agrobacterium strain carrying the mTagBFP2-HA-AtPEX11E construct. To obtain *pex11cde* expressing mTagBFP2-HA-AtPEX11B, *pex11c/c d/d E/e* plants were transformed, and homozygous *pex11cde* mutants expressing mTagBFP2-HA-AtPEX11B were obtained from the progeny of the original transformants. Transgenic plants containing mTagBFP2-HA-PEX11 variants were confirmed via PCR-based genotyping (Supplementary Table 5).

CRISPR-Cas9 mutagenesis and genotyping

Transformants containing a CRISPR-Cas9-gRNA construct were selected as red fluorescent (from the pOLE1-tRFP on the Cas9 transgene) T_1 seeds and genotyped by PCR-amplifying the targeted region from cauline leaves. Amplicons were Sanger-sequenced (Azenta/Genewiz) to identify plants with mutations of interest. In the next generation, non-red-fluorescent T_2 seeds (lacking the Cas9 transgene) were selected, and T_2 plants were genotyped by Sanger sequencing of PCR amplicons (Supplementary Table 6).

DNA was extracted from seedlings or leaves for genotyping by placing a cauline leaf or multiple seedlings into 8-well PCR strip tubes. 25 µL of 50 mM NaOH was added to each tube and incubated for 15 min at 100 °C. 25 µL of neutralization buffer (200 mM Tris, 1 mM EDTA, pH 8.0) was added to each tube, tissue was dispersed into the solution using pipette tips on a mutli-channel pipette, and 2.5 uL was used as PCR template.

To confirm genotypes of seed stocks, DNA was extracted from seeds using a modified protocol[115,116]. Approximately 100 seeds were frozen on dry ice and ground before adding 200 µL Edwards buffer (200 mM Tris-HCl pH 7.5, 250 mM NaCl, 25 mM EDTA, and 0.5% SDS). Samples were centrifuged for 5 minutes at 15,800 x g, and the supernatant was transferred to a new tube before adding 200 µL of isopropanol. Samples were mixed by inversion and then centrifuged at 15,800 x g for 5 minutes. Pellets were dissolved in 100 µL H_2O, and 1-2 µL was used as PCR template.

Microscopy

To screen for mTagBFP2 expression in seedlings or to screen for the Cas9 transgene via pOLE1-tRFP in seeds, fluorescence was detected using a Leica MZ10F fluorescence stereomicroscope with band-pass filters for ET Blue, GFP3, and ET DsRed.

Live-cell confocal scanning microscopy imaging experiments used seedlings grown on PNS unless otherwise noted. For lipid mobilization inhibition experiments, seedlings were grown vertically on PNS supplemented with 25 µM DMP (from a 50 mM stock in DMSO) or PNS supplemented with the same volume of DMSO (mock) for 3 days before imaging. To image *pxa1* mutants, seed coats were gently nicked (after stratification but before plating) using tweezers to promote germination. To induce tagged-PEX11 expression in *pex11* mutants, seedlings with and without the PEX11 transgene were grown vertically on PNS supplemented with 25 µM β-estradiol (from a 100 mM stock in DMSO) for 3 days before imaging. To image peroxisomes in *pex11* quintuple mutants, seedlings from a *pex11a/a b/b c/c d/d E/e* parent were imaged and then genotyped to identify quintuple mutant seedlings.

To stain lipid droplets, seedlings were incubated in microcentrifuge tubes containing 100 µM monodansylpentane (Abcepta, SM1000b) in 50 mM Tris-HCl (pH 7.6) for at least 20 minutes with rocking.

For confocal imaging, seedlings were mounted in water or lipid droplet dye solution on glass slides (VWR, 48311-951) with 0.16-mm coverslips (VWR, 48393-241). For time-lapse imaging, seedling hypocotyls were excised, placed onto Lab-Tek II 2-well chamber slides (ThermoFisher, 155379), and overlaid with a thin layer of PN with 0.6% agar for imaging.

Fluorescence was captured using an Olympus FV3000RS inverted laser scanning confocal microscope equipped with FV31S-SW Fluoview Acquisition software (version 2.6.1.243) and multialkali spectral GaAsP detectors. An UPLXAPO 60x/1.42 oil-immersion objective was used for imaging experiments except Fig. 1b, which used an UPLXAPO 10X/0.40 objective.

When imaging two reporters, mNeonGreen was excited with a 488-nm laser and emission was captured between 500-540 nm, and mRuby3 was excited with a 561-nm laser and emission was captured between 570-620 nm. Each channel was imaged on separate imaging tracks with the brightfield channel imaged simultaneously with mRuby3.

When imaging three reporters or two reporters and lipid droplet dye, mTagBFP2 or monodansylpentane was excited with a 405-nm laser and emission was captured between 412-475 nm, mNeonGreen was excited with a 488-nm laser and emission was captured between 500-540 nm, and mRuby3 was excited with a 561-nm laser and emission was captured between 571-612 nm. Each channel was imaged on separate imaging tracks with the brightfield channel imaged simultaneously with mNeonGreen.

All images were acquired as z-stacks. Images were displayed as a single slice from a z-stack or as maximum-intensity projections. All imaging was done with sequential line scanning with no line averaging. Images were acquired with 16-bit depth at 1024 ×1024 resolution.

At least three seedlings of each genotype from each time point or condition were imaged for each experiment. Selected confocal images represent events that were observed in multiple cells from at least three different seedlings in the T_2 or T_3 generation. For imaging experiments with *pex11ab* expressing mTagBFP2-HA-PEX11E,

8 seedlings were observed that had varying effects on peroxisome morphology, which appears to be influenced by the amount of mTagBFP2-HA-PEX11E. Three images were selected to represent the effects of varied levels of mTagBFP2-HA-PEX11E.

Image analysis and peroxisome quantification

Orthogonal representations of cotyledon peroxisomes were generated in FIJI using files trimmed to contain 16 slices acquired using 3-μm steps.

To quantify peroxisome size and number, images from three seedlings were analyzed for each condition. The peroxisome membrane (green) channel was used to enable inclusion of both pre-peroxisomes (lacking the lumenal marker) and mature peroxisomes (enclosing the lumenal marker). For quantifying peroxisomes in mock- or DMP-treated seedling hypocotyls (Fig. 4b, c, Supplementary Fig. 4c), 160 ×80 μm regions of the peroxisome membrane channel were used to generate maximum-intensity projections from 10 slices with 1-μm steps. For quantifying peroxisomes in cotyledons (Figs. 1d–h and 7d, e), 120 ×120 μm regions of the peroxisome membrane channel were quantified using maximum-intensity projections from 10 slices with 1-μm steps [Fig. 1 (2-, 3-, and 5-day time points); Fig. 7] or 10 slices with 3-μm steps [Fig. 1 (7-day time point)]. FIJI was used to generate maximum-intensity projections, and the oval tool was used to manually outline peroxisomes, count peroxisomes, and calculate areas. Peroxisomes on the border of an image were included if the peroxisome appeared to be spherical and >50% of the peroxisome area was included. Microsoft Excel was used to calculate diameter from area. Peroxisomes that appeared to be moving excessively (based on examination of the z-stack files) and peroxisome clusters containing ambiguous individual peroxisomes outlines were counted but were excluded from diameter calculations. For peroxisome size stacked bar charts, peroxisome diameters for each time point were binned by size, converted to percentages, and the mean of three replicate percentages was plotted. To account for the 3-fold larger step size for the 7-day time point in Fig. 1, peroxisome numbers were normalized by dividing by 3. To calculate total peroxisome volume, the mean peroxisome diameter from each replicate was converted into spherical volume, multiplied by the number of peroxisomes for that replicate, and normalized to the mean wild-type peroxisome volume at 2 days.

Immunoblotting

Seedlings grown on PNS medium (physiological assays) or PNS supplemented with 25 μM β-estradiol (complementation experiments) were frozen on dry ice and stored at −80 °C until processing. Protein was extracted from ground, frozen plant tissue by adding 3 volumes of sample buffer [435 mM Tris pH 8.5, 3.5% (w/v) lithium dodecyl sulfate, 870 μM EDTA, 17.4% (w/v) glycerol, 48 μM Coomassie blue G250, and 65 mM dithiothreitol] and then incubating the samples at 100 °C for 5 min. The samples were centrifuged at 18,500 x g for 5 min at 4 °C, and then equal volumes of supernatants were loaded on Bolt 10% (w/v) polyacrylamide Bis-Tris gels (Invitrogen) alongside diluted pre-stained markers (New England Biolabs, P7719). The gels were electrophoresed in MOPS running buffer [50 mM MOPS, 50 mM Tris pH 7.7, 1 mM EDTA, 0.1% (w/v) SDS] containing a 1:400 dilution of NuPAGE Antioxidant (Invitrogen). The proteins were transferred from the gel to Hybond-ECL nitrocellulose membranes (Amersham, Protran Premium 0.45 μm NC; 10600003) using a GenScript eBlot L1 transfer system (GenScript, L00686). Membranes were air-dried overnight before blocking for at least 1 hour at room temperature with 8% (w/v) nonfat dry milk in TBST [20 mM Tris pH 7.5, 150 mM NaCl, 0.1% (v/v) Tween-20]. After blocking, membranes were incubated at 4 °C with primary antibodies diluted in 8% milk in TBST for at least 1 day with rocking. Primary antibodies were mouse anti-HSC70 (1:50,000; Stressgen SPA-817), rat anti-HA (1:100; Sigma 11867431001 Roche 3F10), rabbit anti-PEX11E[46] (1:1000), rabbit anti-PEX14 (1:10,000; Agrisera AS08 372), rabbit anti-PMDH2[84] (1:10,000), or rabbit anti-OLE1 (1:2000; Cedarlane CLAS20-4412). After incubation with primary antibodies, membranes were washed three times for 5 minutes in TBST and then incubated with secondary antibodies diluted in 8% milk in TBST for at least 1 hour at room temperature. Secondary antibodies were horseradish-peroxidase (HRP)-linked goat anti-mouse (1:2500 or 1:5000; Invitrogen 31430), goat anti-rat (1:1000; Invitrogen A10549), or goat anti-rabbit (1:2500 or 1:5000; LI-COR 926-80011). Membranes were imaged with WesternSure Premium Chemiluminescent substrate (LI-COR, 926-95000) using an Odyssey Fc imaging system (LI-COR, 2801-02). Membranes were sequentially probed with primary antibodies recognizing proteins of different sizes without stripping. Quantification was performed using Image Studio software (LI-COR, version 5.2).

Lipid analysis

TAG levels were monitored by thin-layer chromatography (TLC). 5 mg of seeds were plated on PNS in triplicate for each genotype and time point and harvested after 3, 5, or 7 days, frozen on dry ice, and stored at −80 °C. Lipids were extracted using a modified Folch extraction method[6,117]. Tissue was ground in 1.7 mL microcentrifuge tubes after being frozen in liquid nitrogen. 500 μL of methanol/chloroform/formic acid (2:1:0.1, v/v/v) was added to ground sample and vortexed for 10 minutes at room temperature. 250 μL of phase separation solution (1 M KCl, 0.2 M H_3PO_4) was added. Samples were vortexed, then centrifuged at 18,000 x g for 5 minutes at room temperature. Equal volumes of the lower phase were spotted onto TLC plates (silica gel 60, Sigma, 1.05721 plates) and placed into a glass chamber containing a mobile phase consisting of hexane/diethyl ether/acetic acid (70:30:1, v/v/v). TAG was visualized by dipping plates into 5.0% H_2SO_4, drying until water evaporated, and heating at approximately 100 °C for 5-10 minutes until color developed. For TAG quantification, TLC plates were scanned using a flatbed scanner and converted into 32-bit grayscale TIF images, which were quantified using Image Studio software (LI-COR).

For lipidomic analysis, approximately 40-50 mg of seeds for each genotype were plated on PNS plates for each time point. Five replicates of 5-40 mg of seedling tissue were harvested at 3, 7, and 12 days, frozen in liquid nitrogen, and stored at −80 °C. Lipidomics analysis was performed by the Kansas Lipidomics Research Center (Manhattan, KS)[118] to monitor 359 lipids. Harvested seedlings were transferred to a vial containing 0.8 ml isopropanol with 0.01% BHT preheated to 75 °C and incubated for 15 min. Lipids were extracted by shaking at room temperature for 24 h after adding 2.4 mL of chloroform/methanol/water (40:55:5, v/v/v). The seedling tissue was removed to a new vial, dried, and weighed. The volume of extracted lipid corresponding to 0.085 mg dry tissue was evaporated and dissolved in 300 μL chloroform/methanol/300 mM ammonium acetate in water (30:66.5:3.5, v/v/v) along with internal standards for direct-infusion electrospray ionization tandem mass spectrometry analysis using a Sciex 6500+ mass spectrometer. Quality control samples, which were identical pooled samples containing internal standards, and internal-standard-only samples were placed at regular intervals among the experimental samples[118]. In positive mode, the ion spray voltage was 5500 V, the curtain gas was 35 psi, the source temperature was 100 °C, the ion source gas (GAS1) was 45 psi, the ion source gas (GAS2) was 45 psi, the declustering potential was 100 V, and the entrance potential was 10 V. In negative mode, parameters were the same except the ion spray voltage was −4500 V, the declustering potential was −100 V, and the entrance potential was −10 V. The collision gas was nitrogen[118]. Multiple reaction monitoring (MRM) data were processed and exported to Excel using MultiQuant software (version 3.0.2). Lipids were targeted based on the masses of intact ions (m/z) and individual fragment ions. Data were quantified using LipidomeDB Data Calculation Environment (http://lipidome.bcf.ku.edu:8080/Lipidomics/). No response factors were used in the quantification; 1 nmol = the amount of lipid that produced the same mass spectral intensity as 1 nmol of the best-

matched internal standard. The 203 lipids with a coefficient of variation less than 0.3 (calculated from repeated infusion of the quality control samples throughout the analysis) and that were present above the detection limit of 0.0005 nmol for the mean of pooled replicate samples were included in the quantitative analyses (Supplementary Data 1). Data were processed and visualized using the "ggplot2" and "tidyverse" packages in RStudio (version 2025.05.1 + 513). For principal component analysis, the data were normalized using the Z-score method in RStudio. For bar and stacked bar charts, the percentages of total lipid content for each lipid type were summed, and the means of the five biological replicates were plotted.

Statistical analysis

Statistical tests were performed using JMP Student Edition (version 18.2.1). For the adult plant survival plot, the Mantel-Cox (log-rank) test was performed to compare the difference in survival curves using pairwise comparison between each genotype and the wild-type reporter utilizing Bonferroni correction to adjust p-values. Two-tailed t tests were used to compare peroxisome diameter of DMP-treated seedlings. Chi-square analysis with Pearson's test was used to show that the *pex11a/a b/b c/c d/d e/e* mutations did not confer embryonic lethality. One-way ANOVA was performed to compare peroxisome diameter, number, and volume; sucrose dependence; IBA responsiveness; rosette diameter; PMDH processing and OLE1 levels; TAG levels in *pex11* mutant time course TLC assays; and percentages of total lipid content for each lipid type. When p-values were <0.05, Tukey's post hoc test was used to compare means and assign homogenous subsets. For lipidomics volcano plots, one-factor statistical analysis and probabilistic quotient normalization to the wild-type reporter line were performed in MetaboAnalyst 6.0, and the resultant fold-changes and p-values were exported for visualization in RStudio. Data graphed using GraphPad Prism or RStudio were imported into Adobe Illustrator (version 29.8.1) for figure assembly.

Reporting summary

Further information on research design is available in the Nature Portfolio Reporting Summary linked to this article.

Data availability

The data supporting the findings of the study are available within the main text or supplementary information. Source data are provided with the paper. Source data are provided with this paper.

References

1. Kao, Y.-T., Gonzalez, K. L. & Bartel, B. Peroxisome Function, Biogenesis, and Dynamics in Plants. *Plant Physiol.* **176**, 162–177 (2018).
2. Nagan, N. & Zoeller, R. A. Plasmalogens: biosynthesis and functions. *Prog. Lipid Res.* **40**, 199–229 (2001).
3. Steinberg, S. J. et al. Peroxisome biogenesis disorders. *Biochimica et. Biophysica Acta (BBA) - Mol. Cell Res.* **1763**, 1733–1748 (2006).
4. Braverman, N. E. et al. Peroxisome biogenesis disorders in the Zellweger spectrum: An overview of current diagnosis, clinical manifestations, and treatment guidelines. *Mol. Genet. Metab.* **117**, 313–321 (2016).
5. Hoepfner, D., Schildknegt, D., Braakman, I., Philippsen, P. & Tabak, H. F. Contribution of the endoplasmic reticulum to peroxisome formation. *Cell* **122**, 85–95 (2005).
6. Wright, Z. J., Tharp, N. E. & Bartel, B. ER nests are specialized ER subdomains in Arabidopsis where peroxisomes and lipid droplets form. *Developmental Cell* **60**, 2061–2080.e4 (2025).
7. Lazarow, P. B. & Fujiki, Y. Biogenesis of Peroxisomes. *Annu. Rev. Cell Developmental Biol.* **1**, 489–530 (1985).
8. Titorenko, V. I. & Mullen, R. T. Peroxisome biogenesis: the peroxisomal endomembrane system and the role of the ER. *J. Cell Biol.* **174**, 11–17 (2006).
9. Schrader, T. A. et al. PEX11β and FIS1 cooperate in peroxisome division independently of mitochondrial fission factor. *J. Cell Sci.* **135**, jcs259924 (2022).
10. Jansen, R. L. M., Santana-Molina, C., van den Noort, M., Devos, D. P. & van der Klei, I. J. Comparative Genomics of Peroxisome Biogenesis Proteins: Making Sense of the PEX Proteins. *Front. Cell Dev. Biol.* **9**, (2021).
11. Smith, J. J. & Aitchison, J. D. Peroxisomes take shape. *Nat. Rev. Mol. Cell Biol.* **14**, 803–817 (2013).
12. Skowyra, M. L., Feng, P. & Rapoport, T. A. Towards solving the mystery of peroxisomal matrix protein import. *Trends Cell Biol.* **34**, 388–405 (2024).
13. Koch, J. et al. PEX11 family members are membrane elongation factors that coordinate peroxisome proliferation and maintenance. *J. Cell Sci.* **123**, 3389–3400 (2010).
14. Opaliński, Ł, Kiel, J. A. K. W., Williams, C., Veenhuis, M. & van der Klei, I. J. Membrane curvature during peroxisome fission requires Pex11. *EMBO J.* **30**, 5–16 (2011).
15. Thoms, S. & Erdmann, R. Dynamin-related proteins and Pex11 proteins in peroxisome division and proliferation. *FEBS J.* **272**, 5169–5181 (2005).
16. Lingard, M. J. et al. Arabidopsis PEROXIN11c-e, FISSION1b, and DYNAMIN-RELATED PROTEIN3A Cooperate in Cell Cycle–Associated Replication of Peroxisomes. *Plant Cell* **20**, 1567–1585 (2008).
17. Aung, K. & Hu, J. Differential roles of Arabidopsis dynamin-related proteins DRP3A, DRP3B, and DRP5B in organelle division. *J. Integr. Plant Biol.* **54**, 921–931 (2012).
18. Williams, C. et al. The membrane remodeling protein Pex11p activates the GTPase Dnm1p during peroxisomal fission. *Proc. Natl. Acad. Sci.* **112**, 6377–6382 (2015).
19. Erdmann, R. & Blobel, G. Giant peroxisomes in oleic acid-induced Saccharomyces cerevisiae lacking the peroxisomal membrane protein Pmp27p. *J. Cell Biol.* **128**, 509–523 (1995).
20. Rottensteiner, H., Stein, K., Sonnenhol, E. & Erdmann, R. Conserved Function of Pex11p and the Novel Pex25p and Pex27p in Peroxisome Biogenesis. *MBoC* **14**, 4316–4328 (2003).
21. Kamisugi, Y. et al. Giant peroxisomes in a moss (Physcomitrella patens) peroxisomal biogenesis factor 11 mutant. *N. Phytologist* **209**, 576–589 (2016).
22. Nito, K., Kamigaki, A., Kondo, M., Hayashi, M. & Nishimura, M. Functional Classification of Arabidopsis Peroxisome Biogenesis Factors Proposed from Analyses of Knockdown Mutants. *Plant Cell Physiol.* **48**, 763–774 (2007).
23. Orth, T. et al. The PEROXIN11 protein family controls peroxisome proliferation in Arabidopsis. *Plant Cell* **19**, 333–350 (2007).
24. Schrader, M. et al. Expression of PEX11beta mediates peroxisome proliferation in the absence of extracellular stimuli. *J. Biol. Chem.* **273**, 29607–29614 (1998).
25. Li, X. & Gould, S. J. PEX11 promotes peroxisome division independently of peroxisome metabolism. *J. Cell Biol.* **156**, 643–651 (2002).
26. Yoshida, Y., Niwa, H., Honsho, M., Itoyama, A. & Fujiki, Y. Pex11 mediates peroxisomal proliferation by promoting deformation of the lipid membrane. *Biol. Open* **4**, 710–721 (2015).
27. Lingard, M. J. & Trelease, R. N. Five Arabidopsis peroxin 11 homologs individually promote peroxisome elongation, duplication or aggregation. *J. Cell Sci.* **119**, 1961–1972 (2006).
28. Marshall, P. A. et al. Pmp27 promotes peroxisomal proliferation. *J. Cell Biol.* **129**, 345–355 (1995).
29. Chang, J. et al. An ancestral role in peroxisome assembly is retained by the divisional peroxin Pex11 in the yeast Yarrowia lipolytica. *J. Cell Sci.* **128**, 1327–1340 (2015).
30. Li, X. et al. PEX11 beta deficiency is lethal and impairs neuronal migration but does not abrogate peroxisome function. *Mol. Cell Biol.* **22**, 4358–4365 (2002).

31. Asare, A., Levorse, J. & Fuchs, E. Coupling organelle inheritance with mitosis to balance growth and differentiation. *Science* **355**, eaah4701 (2017).
32. Li, X. et al. PEX11alpha is required for peroxisome proliferation in response to 4-phenylbutyrate but is dispensable for peroxisome proliferator-activated receptor alpha-mediated peroxisome proliferation. *Mol. Cell Biol.* **22**, 8226–8240 (2002).
33. Gruber, P. J., Trelease, R. N., Becker, W. M. & Newcomb, E. H. A correlative ultrastructural and enzymatic study of cotyledonary microbodies following germination of fat-storing seeds. *Planta* **93**, 269–288 (1970).
34. Trelease, R. N., Becker, W. M., Gruber, P. J. & Newcomb, E. H. Microbodies (Glyoxysomes and Peroxisomes) in Cucumber Cotyledons: Correlative Biochemical and Ultrastructural Study in Light- and Dark-Grown Seedlings. *Plant Physiol.* **48**, 461–475 (1971).
35. Wanner, G., Vigil, E. L. & Theimer, R. R. Ontogeny of microbodies (glyoxysomes) in cotyledons of dark-grown watermelon (Citrullus vulgaris Schrad.) seedlings. *Planta* **156**, 314–325 (1982).
36. Wright, Z. J. & Bartel, B. Peroxisomes form intralumenal vesicles with roles in fatty acid catabolism and protein compartmentalization in Arabidopsis. *Nat. Commun.* **11**, 6221 (2020).
37. McNew, J. A. & Goodman, J. M. An oligomeric protein is imported into peroxisomes in vivo. *J. Cell Biol.* **127**, 1245–1257 (1994).
38. Stevens, P. et al. Hansenula polymorpha Vam7p is required for macropexophagy. *FEMS Yeast Res.* **5**, 985–997 (2005).
39. Gorgas, K. & Krisans, S. K. Zonal heterogeneity of peroxisome proliferation and morphology in rat liver after gemfibrozil treatment. *J. Lipid Res* **30**, 1859–1875 (1989).
40. Hashiguchi, N. et al. Peroxisomes Are Formed from Complex Membrane Structures in PEX6-deficient CHO Cells upon Genetic Complementation. *Mol. Biol. Cell* **13**, 711–722 (2002).
41. Rinaldi, M. A. et al. The Roles of β-Oxidation and Cofactor Homeostasis in Peroxisome Distribution and Function in Arabidopsis thaliana. *Genetics* **204**, 1089–1115 (2016).
42. Bartel, B., Burkhart, S. E. & Fleming, W. A. Protein Transport In and Out of Plant Peroxisomes. in *Molecular Machines Involved in Peroxisome Biogenesis and Maintenance* (eds Brocard, C. & Hartig, A.) 325–345 (Springer, Vienna, 2014). https://doi.org/10.1007/978-3-7091-1788-0_14.
43. Gu, Y., Alam, S. & Oliferenko, S. Peroxisomal compartmentalization of amino acid biosynthesis reactions imposes an upper limit on compartment size. *Nat. Commun.* **14**, 5544 (2023).
44. Huang, S. et al. The plant ESCRT component FREE1 regulates peroxisome-mediated turnover of lipid droplets in germinating Arabidopsis seedlings. *The Plant Cell* koac195 https://doi.org/10.1093/plcell/koac195 (2022).
45. Grützner, R. et al. High-efficiency genome editing in plants mediated by a Cas9 gene containing multiple introns. *Plant Commun.* **2**, 100135 (2021).
46. Mitsuya, S. et al. Salt Stress Causes Peroxisome Proliferation, but Inducing Peroxisome Proliferation Does Not Improve NaCl Tolerance in Arabidopsis thaliana. *PLOS ONE* **5**, e9408 (2010).
47. Monroe-Augustus, M. et al. Matrix proteins are inefficiently imported into Arabidopsis peroxisomes lacking the receptor-docking peroxin PEX14. *Plant Mol. Biol.* **77**, 1–15 (2011).
48. Helm, M. et al. Dual specificities of the glyoxysomal/peroxisomal processing protease Deg15 in higher plants. *Proc. Natl. Acad. Sci. USA* **104**, 11501–11506 (2007).
49. Schuhmann, H., Huesgen, P. F., Gietl, C. & Adamska, I. The DEG15 serine protease cleaves peroxisomal targeting signal 2-containing proteins in Arabidopsis. *Plant Physiol.* **148**, 1847–1856 (2008).
50. Lingard, M. J. & Bartel, B. Arabidopsis LON2 Is Necessary for Peroxisomal Function and Sustained Matrix Protein Import. *Plant Physiol.* **151**, 1354–1365 (2009).
51. Hu, J. et al. Plant Peroxisomes: Biogenesis and Function. *Plant Cell* **24**, 2279–2303 (2012).
52. Hayashi, M., Toriyama, K., Kondo, M. & Nishimura, M. 2,4-Dichlorophenoxybutyric Acid–Resistant Mutants of Arabidopsis Have Defects in Glyoxysomal Fatty Acid β-Oxidation. *Plant Cell* **10**, 183–195 (1998).
53. Zolman, B. K., Yoder, A. & Bartel, B. Genetic Analysis of Indole-3-butyric Acid Responses in Arabidopsis thaliana Reveals Four Mutant Classes. *Genetics* **156**, 1323–1337 (2000).
54. Strader, L. C. et al. Multiple facets of Arabidopsis seedling development require indole-3-butyric acid-derived auxin. *Plant Cell* **23**, 984–999 (2011).
55. Eastmond, P. J. SUGAR-DEPENDENT1 encodes a patatin domain triacylglycerol lipase that initiates storage oil breakdown in germinating arabidopsis seeds. *Plant Cell* **18**, 665–675 (2006).
56. Germain, V. et al. Requirement for 3-ketoacyl-CoA thiolase-2 in peroxisome development, fatty acid β-oxidation and breakdown of triacylglycerol in lipid bodies of Arabidopsis seedlings. *Plant J.* **28**, 1–12 (2001).
57. Pinfield-Wells, H. et al. Sucrose rescues seedling establishment but not germination of Arabidopsis mutants disrupted in peroxisomal fatty acid catabolism. *Plant J.* **43**, 861–872 (2005).
58. Deruyffelaere, C. et al. Ubiquitin-mediated proteasomal degradation of oleosins is involved in oil body mobilization during post-germinative seedling growth in Arabidopsis. *Plant Cell Physiol.* **56**, 1374–1387 (2015).
59. Traver, M. S. & Bartel, B. The ubiquitin-protein ligase MIEL1 localizes to peroxisomes to promote seedling oleosin degradation and lipid droplet mobilization. *Proc. Natl. Acad. Sci. USA* **120**, e2304870120 (2023).
60. Brown, L.-A. et al. An inhibitor of oil body mobilization in Arabidopsis. *N. Phytologist* **200**, 641–649 (2013).
61. Zolman, B. K., Silva, I. D. & Bartel, B. The Arabidopsis pxa1 Mutant Is Defective in an ATP-binding cassette transporter-like protein required for peroxisomal fatty acid β-oxidation. *Plant Physiol.* **127**, 1266–1278 (2001).
62. Footitt, S. et al. Control of germination and lipid mobilization by COMATOSE, the Arabidopsis homologue of human ALDP. *EMBO J.* **21**, 2912–2922 (2002).
63. Kelly, A. A., Quettier, A.-L., Shaw, E. & Eastmond, P. J. Seed Storage Oil Mobilization Is Important But Not Essential for Germination or Seedling Establishment in Arabidopsis. *Plant Physiol.* **157**, 866–875 (2011).
64. Pogson, B. J., Ganguly, D. & Albrecht-Borth, V. Insights into chloroplast biogenesis and development. *Biochimica et. Biophysica Acta (BBA) - Bioenerg.* **1847**, 1017–1024 (2015).
65. Pierre-Jerome, E., Drapek, C. & Benfey, P. N. Regulation of Division and Differentiation of Plant Stem Cells. *Annu Rev. Cell Dev. Biol.* **34**, 289–310 (2018).
66. Klepikova, A. V., Kasianov, A. S., Gerasimov, E. S., Logacheva, M. D. & Penin, A. A. A high resolution map of the Arabidopsis thaliana developmental transcriptome based on RNA-seq profiling. *Plant J.* **88**, 1058–1070 (2016).
67. Zuo, J., Niu, Q.-W. & Chua, N.-H. An estrogen receptor-based transactivator XVE mediates highly inducible gene expression in transgenic plants. *Plant J.* **24**, 265–273 (2000).
68. Schumann, U., Wanner, G., Veenhuis, M., Schmid, M. & Gietl, C. AthPEX10, a nuclear gene essential for peroxisome and storage organelle formation during Arabidopsis embryogenesis. *Proc. Natl. Acad. Sci. USA* **100**, 9626–9631 (2003).
69. Sparkes, I. A. et al. An Arabidopsis pex10 Null Mutant Is Embryo Lethal, Implicating Peroxisomes in an Essential Role during Plant Embryogenesis. *Plant Physiol.* **133**, 1809–1819 (2003).

70. Fan, J. et al. The Arabidopsis PEX12 gene is required for peroxisome biogenesis and is essential for development. *Plant Physiol.* **139**, 231–239 (2005).
71. Prestele, J. et al. Different functions of the C3HC4 zinc RING finger peroxins PEX10, PEX2, and PEX12 in peroxisome formation and matrix protein import. *Proc. Natl. Acad. Sci. USA* **107**, 14915–14920 (2010).
72. Rinaldi, M. A. et al. The PEX1 ATPase stabilizes PEX6 and plays essential roles in peroxisome biology. *Plant Physiol.* **174**, 2231–2247 (2017).
73. Buck, G. C., Weeks, A. D., Ordner, N. E. & Bartel, B. Identifying and characterizing a missing peroxin—PEX8—in Arabidopsis thaliana. *Plant Cell* **37**, koaf166 (2025).
74. Torii, K. U. Stomatal Patterning and Guard Cell Differentiation. in *Cell Division Control in Plants* (eds Verma, D. P. S. & Hong, Z.) 343–359 (Springer, Berlin, Heidelberg, 2008). https://doi.org/10.1007/7089_2007_135.
75. Mindthoff, S. et al. Peroxisomal Pex11 is a pore-forming protein homologous to TRPM channels. *Biochimica et. Biophysica Acta (BBA) - Mol. Cell Res.* **1863**, 271–283 (2016).
76. Theodoulou, F. L., Carrier, D. J., Schaedler, T. A., Baldwin, S. A. & Baker, A. How to move an amphipathic molecule across a lipid bilayer: different mechanisms for different ABC transporters?. *Biochem. Soc. Trans.* **44**, 774–782 (2016).
77. Esnay, N., Dyer, J. M., Mullen, R. T. & Chapman, K. D. Lipid Droplet–Peroxisome Connections in Plants. *Contact* **3**, 2515256420908765 (2020).
78. Ralston, A. W. & Hoerr, C. W. THE SOLUBILITIES OF THE NORMAL SATURATED FATTY ACIDS. *J. Org. Chem.* **07**, 546–555 (1942).
79. Chapman, K. D. & Trelease, R. N. Acquisition of membrane lipids by differentiating glyoxysomes: role of lipid bodies. *J. Cell Biol.* **115**, 995–1007 (1991).
80. Bánhegyi, G. et al. Fatty acyl-CoA esters and the permeability of rat liver microsomal vesicles. *Biochem J.* **320**, 343–344 (1996).
81. Wangler, M. F. et al. Peroxisomal biogenesis is genetically and biochemically linked to carbohydrate metabolism in Drosophila and mouse. *PLOS Genet.* **13**, e1006825 (2017).
82. Thoms, S., Debelyy, M. O., Nau, K., Meyer, H. E. & Erdmann, R. Lpx1p is a peroxisomal lipase required for normal peroxisome morphology. *FEBS J.* **275**, 504–514 (2008).
83. Yifrach, E. et al. Systematic multi-level analysis of an organelle proteome reveals new peroxisomal functions. *Mol. Syst. Biol.* **18**, e11186 (2022).
84. Muhammad, D. et al. Global impacts of peroxisome and pexophagy dysfunction revealed through multi-omics analyses of lon2 and atg2 mutants. *Plant J.* **120**, 2563–2583 (2024).
85. Flora, Y., Shastri, D. & Bohnert, K. A. Inhibition of peroxisomal protein PRX-11 promotes longevity in *Caenorhabditis elegans* via enhancements to mitochondria. 2025.05.28.656437 Preprint at https://doi.org/10.1101/2025.05.28.656437 (2025).
86. Kim, P. K., Mullen, R. T., Schumann, U. & Lippincott-Schwartz, J. The origin and maintenance of mammalian peroxisomes involves a de novo PEX16-dependent pathway from the ER. *J. Cell Biol.* **173**, 521–532 (2006).
87. Mast, F. D. et al. ESCRT-III is required for scissioning new peroxisomes from the endoplasmic reticulum. *J. Cell Biol.* **217**, 2087–2102 (2018).
88. Lev, S. Non-vesicular lipid transport by lipid-transfer proteins and beyond. *Nat. Rev. Mol. Cell Biol.* **11**, 739–750 (2010).
89. Toulmay, A. & Prinz, W. A. Lipid transfer and signaling at organelle contact sites: the tip of the iceberg. *Curr. Opin. Cell Biol.* **23**, 458–463 (2011).
90. Yuan, W., Akşit, A., de Boer, R., Krikken, A. M. & van der Klei, I. J. Yeast Vps13 is Crucial for Peroxisome Expansion in Cells With Reduced Peroxisome-ER contact sites. *Front. Cell Dev. Biol.* **10**, (2022).
91. Hua, R. et al. VAPs and ACBD5 tether peroxisomes to the ER for peroxisome maintenance and lipid homeostasis. *J. Cell Biol.* **216**, 367–377 (2017).
92. Costello, J. L. et al. ACBD5 and VAPB mediate membrane associations between peroxisomes and the ER. *J. Cell Biol.* **216**, 331–342 (2017).
93. Gao, C. et al. A unique plant ESCRT component, FREE1, regulates multivesicular body protein sorting and plant growth. *Curr. Biol.* **24**, 2556–2563 (2014).
94. Kim, A. S., Wu, J. Z., Cai, R. & Freeman, S. A. Mechanoresilience of lysosomes conferred by TMEM63A. *J. Cell Biol.* **225**, e202509180 (2026).
95. Ebeed, H. T., Stevenson, S. R., Cuming, A. C. & Baker, A. Conserved and differential transcriptional responses of peroxisome associated pathways to drought, dehydration and ABA. *J. Exp. Bot.* **69**, 4971–4985 (2018).
96. Li, J. & Hu, J. Using co-expression analysis and stress-based screens to uncover arabidopsis peroxisomal proteins involved in drought response. *PLoS ONE* **10**, e0137762 (2015).
97. Huber, A., Koch, J., Kragler, F., Brocard, C. & Hartig, A. A subtle interplay between three Pex11 proteins shapes de novo formation and fission of peroxisomes. *Traffic* **13**, 157–167 (2012).
98. Ebberink, M. S. et al. A novel defect of peroxisome division due to a homozygous non-sense mutation in the PEX11β gene. *J. Med. Genet.* **49**, 307–313 (2012).
99. Taylor, R. L. et al. Novel PEX11B mutations extend the peroxisome biogenesis disorder 14B phenotypic spectrum and underscore congenital cataract as an early feature. *Invest Ophthalmol. Vis. Sci.* **58**, 594–603 (2017).
100. Tian, Y. et al. Variant analysis of PEX11B gene from a family with peroxisome biogenesis disorder 14B by whole exome sequencing. *Mol. Genet. Genom. Med.* **8**, (2020).
101. Malekzadeh, H., Shakiba, M. & Yasaei, M. A Novel Mutation in PEX11β Gene. *Iran. J. Child Neurol.* **15**, 93–100 (2021).
102. Khoddam, S. et al. Two siblings with PEX11B-related peroxisome biogenesis disorder. *Eur. J. Med. Genet.* 104928 https://doi.org/10.1016/j.ejmg.2024.104928 (2024).
103. Alonso, J. M. et al. Genome-wide insertional mutagenesis of Arabidopsis thaliana. *Science* **301**, 653–657 (2003).
104. Haughn, G. W. & Somerville, C. Sulfonylurea-resistant mutants of Arabidopsis thaliana. *Molec Gen. Genet.* **204**, 430–434 (1986).
105. Stasinopoulos, T. C. & Hangarter, R. P. Preventing photochemistry in culture media by long-pass light filters alters growth of cultured tissues. *Plant Physiol.* **93**, 1365–1369 (1990).
106. Jumper, J. et al. Highly accurate protein structure prediction with AlphaFold. *Nature* **596**, 583–589 (2021).
107. Varadi, M. et al. AlphaFold Protein Structure Database: massively expanding the structural coverage of protein-sequence space with high-accuracy models. *Nucleic Acids Res.* **50**, D439–D444 (2022).
108. Dobson, L. et al. TmAlphaFold database: membrane localization and evaluation of AlphaFold2 predicted alpha-helical transmembrane protein structures. *Nucleic Acids Res* **51**, D517–D522 (2023).
109. Robert, X. & Gouet, P. Deciphering key features in protein structures with the new ENDscript server. *Nucleic Acids Res.* **42**, W320–W324 (2014).
110. Goddard, T. D. et al. UCSF ChimeraX: Meeting modern challenges in visualization and analysis. *Protein Sci.* **27**, 14–25 (2018).
111. Pettersen, E. F. et al. UCSF ChimeraX: Structure visualization for researchers, educators, and developers. *Protein Sci.* **30**, 70–82 (2021).

112. Labun, K. et al. CHOPCHOP v3: expanding the CRISPR web toolbox beyond genome editing. *Nucleic Acids Res* **47**, W171–W174 (2019).
113. Koncz, C. & Schell, J. The promoter of TL-DNA gene 5 controls the tissue-specific expression of chimaeric genes carried by a novel type of Agrobacterium binary vector. *Molec Gen. Genet* **204**, 383–396 (1986).
114. Clough, S. J. & Bent, A. F. Floral dip: a simplified method for Agrobacterium-mediated transformation of Arabidopsis thaliana. *Plant J.* **16**, 735–743 (1998).
115. Edwards, K., Johnstone, C. & Thompson, C. A simple and rapid method for the preparation of plant genomic DNA for PCR analysis. *Nucleic Acids Res.* **19**, 1349 (1991).
116. Hu, W. & Lagarias, J. C. A one-tube method for rapid and reliable plant genomic DNA isolation for PCR analysis. 2020.02.13.948455 Preprint at https://doi.org/10.1101/2020.02.13.948455 (2020).
117. Yu, L., Fan, J., Zhou, C. & Xu, C. Sterols are required for the coordinated assembly of lipid droplets in developing seeds. *Nat. Commun.* **12**, 5598 (2021).
118. Song, Y. et al. A lipidomic approach to identify cold-induced changes in Arabidopsis membrane lipid composition. *Methods Mol. Biol.* **2156**, 187–202 (2020).

Acknowledgements

We thank Alison Baker for the PEX11E antibody and Gabrielle Buck, Makaela Jackson, Sayuri Jayawardena, Isabella Kreko, Durreshahwar Muhammad, Ana Swearingen, and Cody Upton for useful feedback on the manuscript. We are grateful to Ruth Welti and Mary Roth of the Kansas Lipidomics Research Center Analytical Laboratory for lipidomics analysis and advice. We thank Spencer Freeman for insights on organelle turgor modulation. This work was supported by the National Institutes of Health (R35GM130338 to BB and F31GM150269 to NET), the Robert A. Welch Foundation (C-1309 to BB), a National Science Foundation REU grant 2244041 (to CA), and the American Society of Plant Biologists SURF program (to CA). Lipidomics instrument acquisition and method development were supported by the National Science Foundation (including support from the Major Research Instrumentation program; most recent award DBI-2511193), the USDA National Institute of Food and Agriculture (Hatch/Multi-State project 7001195), and Kansas State University.

Author contributions

N.E.T., Z.J.W., and B.B. conceived and designed the experiments; N.E.T., C.A., J.H., and N.S.S. performed the experiments; N.E.T. and C.A. analyzed the data; and N.E.T, Z.J.W., and B.B. wrote the manuscript with input from all authors.

Competing interests

The authors declare no competing interests.

Additional information

Supplementary information The online version contains supplementary material available at https://doi.org/10.1038/s41467-026-71873-3.

Correspondence and requests for materials should be addressed to Bonnie Bartel.

Peer review information *Nature Communications* thanks Gopal Chowdhary, and the other, anonymous, reviewer(s) for their contribution to the peer review of this work. A peer review file is available.